



**University of
Zurich**^{UZH}

**Zurich Open Repository and
Archive**

University of Zurich
University Library
Strickhofstrasse 39
CH-8057 Zurich
www.zora.uzh.ch

Year: 2018

Distinct in vivo roles of secreted APP ectodomain variants APPs and APPs in regulation of spine density, synaptic plasticity, and cognition

Richter, Max C ; Ludewig, Susann ; Winschel, Alex ; Abel, Tobias ; Bold, Charlotte ; Salzburger, Leonie R ; Klein, Susanne ; Han, Kang ; Weyer, Sascha W ; Fritz, Ann-Kristina ; Laube, Bodo ; Wolfer, David P ; Buchholz, Christian J ; Korte, Martin ; Müller, Ulrike C

Abstract: Increasing evidence suggests that synaptic functions of the amyloid precursor protein (APP), which is key to Alzheimer pathogenesis, may be carried out by its secreted ectodomain (APPs). The specific roles of APPs and APPs fragments, generated by non-amyloidogenic or amyloidogenic APP processing, respectively, remain however unclear. Here, we expressed APPs or APPs in the adult brain of conditional double knockout mice (cDKO) lacking APP and the related APLP2. APPs efficiently rescued deficits in spine density, synaptic plasticity (LTP and PPF), and spatial reference memory of cDKO mice. In contrast, APPs failed to show any detectable effects on synaptic plasticity and spine density. The C-terminal 16 amino acids of APPs (lacking in APPs) proved sufficient to facilitate LTP in a mechanism that depends on functional nicotinic 7-nAChRs. Further, APPs showed high-affinity, allosteric potentiation of heterologously expressed 7-nAChRs in oocytes. Collectively, we identified 7-nAChRs as a crucial physiological receptor specific for APPs and show distinct in vivo roles for APPs versus APPs. This implies that reduced levels of APPs that might occur during Alzheimer pathogenesis cannot be compensated by APPs.

DOI: <https://doi.org/10.15252/embj.201798335>

Posted at the Zurich Open Repository and Archive, University of Zurich

ZORA URL: <https://doi.org/10.5167/uzh-151601>

Journal Article

Accepted Version

Originally published at:

Richter, Max C; Ludewig, Susann; Winschel, Alex; Abel, Tobias; Bold, Charlotte; Salzburger, Leonie R; Klein, Susanne; Han, Kang; Weyer, Sascha W; Fritz, Ann-Kristina; Laube, Bodo; Wolfer, David P; Buchholz, Christian J; Korte, Martin; Müller, Ulrike C (2018). Distinct in vivo roles of secreted APP ectodomain variants APPs and APPs in regulation of spine density, synaptic plasticity, and cognition. EMBO Journal Online, 37(11):e98335.

DOI: <https://doi.org/10.15252/embj.201798335>

Distinct *in vivo* role of APPs α versus APPs β for spine density, synaptic plasticity and cognition

Running Title:

Functions of APPs α and APPs β

Max C. Richter^{1*}, Susann Ludewig^{2*}, Alex Winschel³, Tobias Abel⁴, Charlotte Bold¹, Leonie R. Salzburger², Susanne Klein¹, Kang Han¹, Sascha Weyer¹, Ann-Kristina Fritz⁵, Bodo Laube³, David P. Wolfer⁵, Christian J. Buchholz⁴, Martin Korte^{2, 6} and Ulrike C. Müller^{1#}

¹ Ruprecht-Karls University Heidelberg, Institute of Pharmacy and Molecular Biotechnology (IPMB), Im Neuenheimer Feld 364, 69120 Heidelberg, Germany

² TU Braunschweig, Zoological Institute, Spielmannstraße 7, 38106 Braunschweig, Germany

³ TU Darmstadt, Department of Biology, Neurophysiology und Neurosensory Systems, Schnittspahnstraße 3, 64287 Darmstadt, Germany

⁴ Paul-Ehrlich-Institut (PEI), Paul-Ehrlich-Straße 51-59, 63225 Langen, Germany

⁵ University of Zurich, Institute of Anatomy and ETH Zurich, Institute of Human Movements Sciences and Sport, Winterthurerstraße 190, 8057 Zurich, Switzerland

⁶ Helmholtz Centre for Infection Research, AG NIND, Inhoffenstraße 7, 38124 Braunschweig, Germany

* denotes equal contribution

corresponding author

Key words:

Alzheimer, amyloid precursor protein, soluble APPs α , synaptic plasticity, nicotinic acetylcholine receptor, spines, cognition

Abstract

Increasing evidence suggests that the synaptic functions of the amyloid precursor protein (APP), that is key to Alzheimer pathogenesis, may be carried out by its secreted ectodomain. However, the specific role of APPs fragments generated by non-amyloidogenic or amyloidogenic APP processing remain unclear. Here, we expressed APPs α or APPs β in the adult brain of conditional double knockout mice (cDKO) lacking APP and the related APLP2. APPs α efficiently rescued deficits in spine density, synaptic plasticity (LTP and PPF) and spatial reference memory of cDKO mice. In contrast, APPs β failed to show any detectable effects on synaptic plasticity and spine density. The C-terminal 16 amino acids of APPs α (lacking in APPs β) proved sufficient to facilitate LTP in a mechanism that depends on functional nicotinic $\alpha 7$ -nAChRs. Further, APPs α showed high-affinity, allosteric potentiation of heterologously expressed $\alpha 7$ -nAChRs in oocytes. Collectively, we identified $\alpha 7$ -nAChRs as a crucial physiological receptor specific for APPs α and show distinct *in vivo* roles for APPs α versus APPs β . This implies that reduced levels of APPs α that might occur during Alzheimer pathogenesis cannot be compensated by APPs β .

Introduction

Alzheimer's disease (AD) is characterized by the accumulation of β -amyloid peptides ($A\beta$), that are derived from the amyloid precursor protein (APP) by proteolytic cleavage (Selkoe & Hardy, 2016). Two principal physiological pathways either prevent or promote $A\beta$ generation. Within the amyloidogenic pathway APP processing is shifted towards the production of $A\beta$ and secreted $APPs\beta$, by consecutive β -secretase (BACE1) and γ -secretase cleavage (Vassar et al, 2014). In AD BACE1 is upregulated, favoring amyloidogenic APP processing (Ahmed et al, 2010; Holsinger et al, 2002). In the alternative, non-amyloidogenic pathway cleavage of APP within the $A\beta$ region by the major α -secretase ADAM10 (a disintegrin and metalloprotease) prevents $A\beta$ generation and liberates $APPs\alpha$, that is secreted into the extracellular space (Saftig & Lichtenthaler, 2015). Shifting APP processing towards non-amyloidogenic processing has therefore been suggested as a therapeutic strategy for AD (Mockett et al, 2017). An important and still unresolved question is whether in addition to neurotoxic $A\beta$ accumulation a concomitant reduction in $APPs\alpha$ level, or an altered $APPs\alpha/APPs\beta$ ratio may contribute to AD symptoms and pathogenesis (reviewed by Mockett et al, 2017). In this regard, it will be crucial to know whether $APPs\alpha$ and $APPs\beta$, that is only 16 aminoacids shorter than $APPs\alpha$, serve largely similar or distinct, possibly even opposite physiological functions. While our previous studies and work from others indicated that $APPs\alpha$ has neurotrophic and neuroprotective effects, including synaptogenic, LTP facilitating and memory enhancing properties (Heftner et al, 2016; Hick et al, 2015; Meziane et al, 1998; Milosch et al, 2014; Plummer et al, 2016; Ring et al, 2007; Taylor et al, 2008; Weyer et al, 2014), only few and mostly conflicting studies have as yet addressed the functions of $APPs\beta$ (Chasseigneaux & Allinquant, 2012; Li et al, 2010; Nikolaev et al, 2009; Weyer et al, 2011). So far, the molecular basis of any difference compared to $APPs\alpha$ remained unclear. Thus, a more detailed knowledge about the specific functions of the secreted APP ectodomains is essential to understand AD pathogenesis and evaluate risks of ongoing pharmacotherapy, as well as to elucidate APP physiology.

There is a large body of evidence indicating that APP family proteins are multimodal proteins that can function as ligands via their secreted fragments or as cell surface proteins important for synaptic adhesion and signal transduction (Müller et al, 2017). Major insights into the physiological functions of APP and the related APLPs (APP like proteins) were obtained from knockout models (Müller et al, 2017). While most impairments of APP-KO mice emerged only in aged mice (Dawson et al, 1999; Lee et al, 2010; Ring et al, 2007; Seabrook et al, 1999; Tyan et al, 2012), combined APP/APLP2 double knockout mice die shortly after birth, likely due to severe deficits at the neuromuscular junction (Heber et al, 2000; Klevanski et al, 2014; von Koch et al, 1997; Wang et al, 2005). Recently generated forebrain-specific double knockout mice (termed NexCre cDKO), that lack APP from embryonic day 11.5 onwards in

excitatory forebrain neurons on a global constitutive APLP2-KO background, showed a severe synaptic phenotype already at young age, including reduced spine density and impaired LTP in the hippocampus, as well as deficits in learning and memory (Hick et al, 2015). Interestingly, the LTP impairment of NexCre cDKO mice could be ameliorated by acute APPs α application onto brain slices *in vitro*, while the molecular mechanism and receptor(s) mediating its function remained unknown (Hick et al, 2015).

More recently, we showed that AAV-mediated intracranial expression of APPs α can mitigate the A β related synaptic deficits of APP/PS1 mice *in vivo* (Fol et al, 2016). Intracranial AAV-APPs α injections enhanced spine density, improved LTP deficits and memory, but at the same time also reduced soluble A β levels and plaque load, likely due to enhanced A β clearance (Fol et al, 2016). In addition, APPs α had been reported to lower A β by directly binding to and inhibiting BACE (Obregon et al, 2012). These results raised the question of whether the beneficial *in vivo* effects of APPs α are mainly due to its A β lowering properties.

Here, we asked whether APPs α may also have synaptotrophic effects in an A β independent pathology with synaptic impairments and used viral vectors to express APPs α intracranially in NexCre cDKO mice. Moreover, we set out to compare side-by-side the properties of APPs α and APPs β *in vivo*. We demonstrate that APPs α is sufficient to fully rescue hippocampal spine density, to restore LTP and partially rescue spatial memory in adult NexCre cDKO mice. In sharp contrast, despite similar expression level, APPs β failed to show any detectable effects on synaptic plasticity and spine density. Finally, we show that the CT α 16 domain of APPs α (that is lacking in APPs β) is able to facilitate LTP to the same extent as APPs α , in a mechanism that involves functional nicotinic α 7 acetylcholine receptors (α 7-nAChRs). Moreover, we show that nanomolar concentrations of APPs α (but not APPs β) can directly potentiate α 7-nAChRs-mediated currents upon heterologous expression in *Xenopus* oocytes and increases the apparent agonist affinity as a positive allosteric modulator. Collectively, our analysis identifies the α 7-nAChR as a crucial physiological receptor for APPs α and reveals distinct *in vivo* roles of APPs α versus APPs β .

Materials and Methods

Mice

Experiments on animals were performed in accordance with the guidelines and regulations set forth by the German Animal Welfare Act and the Regierungspräsidium Karlsruhe, Germany. Generation and genotyping of NexCre cDKO mice (further referred as cDKO mice) were as described previously (Hick et al, 2015). Genotype of experimental animals: NexCre cDKO (cDKO), $APP^{flox/flox} APLP2^{-/-} NexCre^{+/T}$ and littermate controls (LM controls), $APP-WT (=APP^{flox/flox}) APLP2^{-/-}$.

AAV plasmid design and vector production

The mouse APP α coding sequence (derived from Uniprot: P12023-2) was codon optimized (Geneart, Germany) and then cloned under control of the synapsin promoter into a single-stranded rAAV2-based shuttle vector, as described previously (Fol et al, 2016). Briefly, the bicistronic DNA constructs harbour a 2A site that connects the cDNA of IckVenus and muAPP α . Venus contains a lymphocyte-specific protein tyrosine kinase (Ick) derived peptide motif which tethers it to the plasma membrane. For easy detection, an N-terminal double HA-tag was inserted downstream of the APP signal peptide (SP) at the N-terminus of APP α . The monocistronic control vector, AAV-Venus, encodes only the yellow fluorescent protein Venus. All constructs were packaged into AAV9 capsids. Briefly, viral particles were produced by transient co-transfection of HEK-293 cells with the transfer vector containing the above-mentioned expression cassettes and the helper plasmid pDP9rs. 72 h following transfection, virions were purified and concentrated from cell lysate and supernatant by ultracentrifugation on a iodixanol density gradient followed by buffer exchange to 0.01% pluronic/phosphate-buffered saline (PBS) via a 100 kDa Amicon centrifugal filter unit. Genome copies in the vector stocks were determined by free inverted terminal repeat (ITR)-specific quantitative TaqMan PCR and expressed as genomic copies per μ l of concentrated stocks (gc/ μ l) as described (D'Costa et al, 2016).

Stereotactic injection of AAVs

Mice were anesthetized by intraperitoneal injection of sleep mix (Medetomidin: 500 μ g/kg, Midazolam: 5 mg/kg, Fentanyl: 50 μ g/kg in isotonic NaCl solution) and positioned on a stereotactic frame (World Precision Instruments, USA). Vector particles (either AAV-Venus, AAV-APP α or AAV-APP β) were injected into the hippocampus at two injection spots per hemisphere using 1 μ l vector stock (titer: 1×10^9 gc/ μ l) per spot at a rate of 0.2 μ l/min. When injection was completed, the cannula was left to rest for 1 min to prevent efflux of viral vector

solution. Stereotactic coordinates of injection sites from bregma were: anteroposterior (A/P): -2 mm, mediolateral (M/L): ± 1 mm, dorsoventral (D/V): -2.25 mm and -1.75 mm. Procedures were approved by the local animal care and use committee (35-9185.81/G-304/14, Regierungspräsidium Karlsruhe, Germany)

Brain samples

Mice were sacrificed 6 weeks post-injection at 5-6 months of age. Following anesthesia, mice were transcardially perfused with PBS before dissection. For immunohistochemistry, one cerebral hemisphere was dissected and post-fixed in 4% paraformaldehyde (PFA) for 48 h and afterwards stored in PBS at 4°C. 40 μ m coronal sections were cut using a vibratome (HM650V Vibratome, Thermo Fisher Scientific, USA) and collected in PBS. The other hemisphere was dissected to segregate hippocampus and cortex for biochemical analysis. Samples were then homogenized using a Polytron homogenizer (Polytron PT-MR 2100, Kinematica AG, Switzerland) in tissue homogenization buffer (THB, 250 mM sucrose, 1 mM EGTA, 20 mM Tris-HCL, pH 7.4) containing 1x protease inhibitor (Complete™ #04693124001, Roche, Switzerland). After centrifugation (10 min, 13,000 rpm, 4°C), the supernatant was collected and the protein concentration was quantified by BCA assay. Lysate aliquots were snap-frozen in liquid N₂ and stored at -80 °C. For the detection of the soluble ectodomain fragments APPs, hippocampal lysates were subjected to high-speed centrifugation (60 min at 100,000x g) and membrane-free supernatant was used for further analysis.

Western blot analysis

Total brain homogenate or supernatant from ultracentrifugation (10 μ g protein) was used for SDS-PAGE. Proteins were separated using 12% Tris-Glycin gels at 20 mA/gel in Laemmli buffer (0.25 M Tris, 2 M glycine and 1% SDS) and transferred to 0.45 μ m PVDF membranes (GE Healthcare, USA) using a tank blot at 450 mA for 1 h (for samples after ultracentrifugation: 450 mA for 1.5 h). After blocking in PBS-T (2.5% Tween in PBS) containing 5% (w/v) dried milk powder at room temperature for 60 min, membranes were incubated with the primary antibodies at 4 °C overnight. The following antibodies were used: α -HA-tag (rabbit, 1:1000, #3724, Cell Signaling Technology, USA was used for total hippocampal homogenates or mouse, 1:1000, #2367, Cell Signaling Technology, USA used for analysis after ultracentrifugation), α -GFAP (rabbit, 1:3000, #173002, Synaptic Systems, Germany), α -Iba1 (rabbit, 1:500, #234003, Synaptic Systems, Germany), α -GFP (chicken, 1:1000, #A10262, Thermo Fisher Scientific, USA), α - β -Tubulin (mouse, 1:10000, #MAB3408, Merck Millipore, USA), M3.2 (mouse, 1:1000, kind gift from Paul Mathews), Y188 (rabbit, 1:1000, #ab32136, Abcam, UK). Membranes were then washed with PBS-T, incubated with a

horseradish peroxidase coupled secondary antibody (goat- α -mouse HRP, 1:10000, #115-165-146, Dianova, Germany; donkey- α -rabbit HRP, 1:10000, #711-035-152, Dianova, Germany; goat- α -chicken HRP, 1:10000, #103-035-155, Dianova, Germany) washed again and developed using SignalFire ECL Reagent (#6883, Cell Signaling Technology, USA) or SignalFire™ Elite ECL Reagent (used for analysis after ultracentrifugation, #12757, Cell Signaling Technology, USA). Signals were detected with the BioRad Chemidoc MP imager (BioRad, Hercules, USA) and analyzed using BioRad Image Lab software.

Immunostaining

Slices were blocked/permeabilized in blocking buffer (5% BSA, 5% NGS, 0.4% Triton X-100 in PBS) overnight at 4°C. To detect AAV-encoded HA-tagged HA-APPs α , slices were incubated with α -HA antibody (rabbit- α -HA, 1:1000, #3724, Cell Signaling Technology, USA or mouse- α -HA, 1:1000, #H3667, Sigma-Aldrich, USA) overnight at 4°C. After three successive washes with PBS-T (2.5% Tween in PBS) slices were incubated in secondary antibody (goat- α -rabbit Cy3, 1:1500, #711-165-152, Jackson ImmunoResearch Laboratories, USA; goat- α -rabbit Cy5, 1:1500, #111-175-144, Jackson ImmunoResearch Laboratories, USA; donkey- α -mouse Cy3, 1:1500, #715-165-150; Jackson ImmunoResearch Laboratories, USA; goat- α -mouse Cy5, 1:1500, #A10524, Thermo Fisher Scientific, USA). For expression analysis HA-APPs α was coimmunostained overnight with the following primary antibodies: α -NeuN (mouse, 1:1500, #MAB377, Merck Millipore, USA), α -GFAP (rabbit, 1:3000, #173002, Synaptic Systems, Germany) and α -Iba1 (rabbit, 1:500, #234003, Synaptic Systems, Germany). Images were taken with a Axio Observer Z1 (Zeiss, Germany) and a Leica TCS SP5II (Leica, Germany).

Electrophysiology

In vitro extracellular recordings were performed on acute hippocampal slices of LM controls stereotactically injected with the AAV-Venus (N=5) and cDKO mice injected either with AAV-Venus (N=4), or AAV-APPs α (N=5). In a separate set of experiments cDKO mice were injected either with AAV-Venus (N=5) or AAV-APPs β (N=5). Investigation of synaptic plasticity was done 7-8 weeks after AAV injection. In-between animals were housed in a temperature- and humidity-controlled room with a 12h light-dark cycle and had access to food and water *ad libitum*.

Slice preparation

Acute hippocampal transversal slices were prepared from isoflurane anesthetized individuals. Following decapitation, the brain was removed and quickly transferred into ice-cold carbogenated (95% O₂, 5% CO₂) artificial cerebrospinal fluid (ACSF) containing

125.0 mM NaCl, 2.0 mM KCl, 1.25 mM NaH₂PO₄, 2.0 mM MgCl₂, 26.0 mM NaHCO₃, 2.0 mM CaCl₂ and 25.0 mM glucose. The hippocampus was sectioned into 400 µm thick transversal slices with a vibrating microtome (VT1200S, Leica, Germany) and maintained in carbogenated ACSF at room temperature for at least 1.5 h. Before recording, each slice of the injected animals was inspected for Venus expression in area CA1 and CA3 (Axiovert 35, Zeiss, Germany). Slices lacking fluorescence in the recording areas were excluded from further analysis.

Peptides and inhibitor

Acute hippocampal slices of LM controls and cDKO mice were pre-incubated in 30 ml gently carbogenated ACSF containing synthetic CT α 16 (DAEFGHDSGFVVRHQK) or a scrambled CT α 16_{scr} peptide (RFDQHGVEDHAFGESK) of the same aminoacid composition as a control. Recombinant recAPPs α was purified from the supernatant of stably transfected HEK cells as described (Hick et al, 2015) and was used at a concentration of 10 nM, in a custom made incubation chamber for 1 h at RT. Afterwards, slices were transferred into the recording chamber where again 30 ml of ACSF with the respective peptide was circulating in a closed loop during the entire experiment. In another set of experiments, the α 7-nicotinic acetylcholine receptor antagonist (α 7-nAChR) α -Bungarotoxin (BTX, Merck Millipore, Germany) solved in *Aqua dest.* was used at a final concentration of 10 nM and either co-applied already at the step of pre-incubation (1h before TBS) together with 10 nM CT α 16 on acute slices or washed in 10 min before baseline recording started.

Extracellular field recordings

Slices were placed in a submerged recording chamber and perfused with carbogenated ACSF (32°C, 125.0 mM NaCl, 2.0 mM KCl, 1.25 mM NaH₂PO₄, 2.0 mM MgCl₂, 26.0 mM NaHCO₃, 2.0 mM CaCl₂ and 25.0 mM glucose) at a rate of 1.2 to 1.5 ml/min. Field excitatory postsynaptic potentials (fEPSPs) were recorded in stratum radiatum of CA1 region with a borosilicate glass micropipette (resistance 2-4 M Ω) filled with 3 M NaCl at a depth of ~150-200 µm. Monopolar tungsten electrodes were used for stimulating the Schaffer collaterals at a frequency of 0.1 Hz. Stimulation intensity was adjusted to ~40% of maximum fEPSP slope for 20 minutes baseline recording. LTP was induced by applying theta-Burst stimulation (TBS: 10 trains of 4 pulses at 100 Hz in an 200 ms interval, repeated 3 times).

Basal synaptic transmission properties were analyzed via input-output (IO) measurements and short-term plasticity was examined via paired pulse facilitation (PPF). The IO-measurements were performed either by application of a defined current values (25-250 µA) or by adjusting the stimulus intensity to certain fiber volley (FV) amplitudes (0.1-0.8 mV). Presynaptic function and short-term plasticity were assessed with the PPF paradigm by

applying a pair of two closely spaced stimuli in inter-stimulus-intervals (ISI) ranging from 10 to 160 ms.

Data analysis and statistics

Data of electrophysiological recordings were collected, stored and analyzed with LABVIEW software (National Instruments, USA). The initial slope of $fEPSPs$ elicited by stimulation of the Schaffer collaterals was measured over time, normalized to baseline and plotted as average \pm SEM. Analysis of the PPF data was performed by calculating the ratio of the slope of the second $fEPSP$ divided by the slope of the first one and multiplied by 100. The statistical analysis was performed using Microsoft Excel or GraphPad Prism version 6.0 (GraphPad, USA). Data obtained between two genotypes or two different experimental conditions were compared using an unpaired two-tailed Student's t -test. Data including more than 2 different groups were analyzed using a one-Way ANOVA followed by a *post-hoc* Bonferroni's Test. All data are indicated as mean \pm SEM. Values of $p < 0.05$ were considered significant and plotted as follows * $p < 0.05$, ** $p < 0.01$, *** $p < 0.001$.

Xenopus Oocyte expression and electrophysiological recording

The rat $\alpha 7$ -nAChR, kindly provided by A. Nicke (Kendel et al, 2013), and the human $\alpha 1$ -GlyR (Laube et al, 2000) cDNAs were subcloned into the oocyte expression vector pNKS2. The original rat $\alpha 7$ -nAChR cDNA had been provided by J. Patrick (Baylor College of Medicine, Houston, USA). The rat $\alpha 7$ -nAChR or the human $\alpha 1$ -GlyR cDNA was linearized and cRNA was synthesized with the SP6 or T7 mMessage mMachine kit, respectively (Ambion, USA). For electrophysiological analysis, *Xenopus laevis* oocytes were injected with 50 ng of the cRNA in a volume of 50 nl. Oocytes were isolated and maintained as described previously (Laube et al, 1997) and approved by the local animal care and use committee (II25.3-19c20/15, RP Darmstadt, Germany). 1-3 days after injection, whole-cell currents were recorded at -70 mV by two-electrode voltage-clamp according to (Laube et al, 2000). Currents were acquired at 200 Hz with a Geneclamp 500B amplifier, a Digidata 1322A digitizer and Clampex 9.2 software (Molecular Devices, USA). The agonists nicotine, acetylcholine or glycine, dissolved in bath solution, was applied either alone for 10 s or after 15 s pre-application of the respective peptides (CT α 16, CT α 16_{scr}, recAPPs α or recAPPs β) also dissolved in bath solution. All experiments were performed at room temperature.

Data analysis and statistics

Currents were measured with Clampfit 9.2 software (Molecular Devices, USA) and results were analyzed using the KaleidaGraph program (Synergy Software, USA) and GraphPad Prism version 6.0 (GraphPad, USA). Peak current responses to nicotine in the absence or presence of APPs α were plotted against agonist concentration and fit with variable slope non-linear regression to establish agonist EC₅₀ parameter (Laube et al, 2000). For peptide modulation, responses to EC₅₀ nicotine (100 μ M), acetylcholine (100 μ M) or glycine (100 μ M) after application were analyzed. Normalized CT α 16-induced fold enhancement of nicotine-induced currents was fit with variable slope non-linear regression (GraphPad Prism version 6.0, GraphPad, USA), yielding EC₅₀ parameters for each individual experiment (Laube et al, 1998). All experiments were from at least two batches of oocytes. Data were compared by paired two-tailed Student's t-test. Values of $p < 0.05$ were considered significant and plotted as follows * $p < 0.05$, ** $p < 0.01$, *** $p < 0.001$. All data are indicated as mean \pm SEM.

Neuronal morphology and spine density

Iontophoretic fillings

In brief, CA1 pyramidal cells were visualized by postfixation filling with Alexa 568 in 200 μ m horizontal brain sections of 5-6 months old mice (see Appendix Table S1 for sex of animals). For iontophoretic fillings of CA1 pyramidal neurons, one brain slice at a time was placed in a custom-made chamber filled with cold PBS and visualized on an Olympus BX51WI fixed stage upright microscope (Olympus, Japan). Sharp quartz glass electrodes (Quartz electrodes with filament, O.D: 1.0 mm, I.D.: 0.7 mm, 10 cm length, Sutter instruments, USA) were pulled using the Sutter P-2000 Laser Puller. The tip of the electrode was loaded with 5 mM Alexa 568 dye dissolved in distilled water and backfilled with 0.1 M LiCl dissolved in distilled water. Using a motorized 3D micromanipulator, the electrode was lowered into the hippocampal CA1 region under visual control using a Calcium Crimson filter cube (HQ580/20x, U-Q595LP (339038), HQ630/60m) while applying a negative voltage pulse (-1 V, 1 Hz) to the electrode via a silver wire in line with a 500 M Ω resistor. When piercing of a cell body was observed, the cell was filled by application of a negative 1 Hz current pulse (~ 5 nA) to the electrode. Filling was for 10 min or until no further filling was observed. Afterwards, slices were fixed for 2 days in 4 % PFA at 4 $^{\circ}$ C, washed three times in cold PBS and finally mounted in Mowiol.

Image acquisition

Images of filled neurons were acquired on a Leica TCS SP5II (Leica, Germany) upright confocal microscope. Overview images of complete neurons used for reconstruction were taken with a 20x objective (Apo 20x/0.75). The complete volume of one filled neuron was imaged with a z-step size of 1 μ m and a 2048 x 2048 resolution. Basal and apical segments

were imaged individually with two overlapping stacks. Detailed images of dendritic segments and spines were acquired using a 63x objective (Apo 63x/1.4 oil) and a digital zoom of 5. To fulfill the Nyquist criteria for deconvolution, z-stacks of dendritic segments were captured with a pixel size of 80 nm and a z-step of 130 nm. Laserpower, gain and offset varied from cell to cell as the parameters were always chosen so that the complete range of the grayscale was used. Images for spine counts were deconvoluted with the AutoQuantX3 software (Media Cybernetics, USA).

Neuronal morphology and spine counts

Filled CA1 pyramidal neurons were manually reconstructed using the Neurolucida software (MicroBrightField, USA) by an experimentator blind to genotype and injected viral vector. Neurons were only included into Sholl analysis if they showed a completely filled apical or basal tree and well defined dendritic endings. The morphometric Sholl analysis was done using the NeuroExplorer software (MicroBrightField, USA). In short, a series of concentric spheres (centered around the soma) was drawn with an intersection interval of 30 μm and the number of dendrites crossing each sphere, as well as the dendritic length in between each sphere was calculated. This analysis was done separately for basal and apical dendrites and was plotted against the distance from the soma. For evaluation of basal dendritic spine density, at least 3 different randomly chosen dendritic segments of the basal dendritic arbour were imaged. They had to fulfil the following criteria: (1) Lie mostly horizontally to the slice surface, (2) be at least 20 μm away from the soma, (3) have a comparable thickness. The minimum basal dendritic length imaged per neuron was 100 μm . For evaluation of midapical dendritic spine density, at least 3 different dendritic segments of the apical tree were imaged. Midapical was defined as the middle third of the length of the apical dendrite measured from the origin of the apical dendrite from the soma to the endpoint of the tufts. Dendritic segments used for evaluation had to fulfil the following criteria: (1) be of second or third order to assure comparable shaft thickness, (2) lie in the middle third of the main apical dendrite (3) be longer than 10 μm . The minimum midapical dendritic length imaged per neuron was 100 μm . Files in the ND2 format were imported into ImageJ (NIH) using the BioFormats Importer. After adjusting, images were saved in the TIFF format. Dendritic spines were manually counted using the Neurolucida and NeuroExplorer software (MicroBrightField, USA) following the criteria of Holtmaat (Holtmaat et al, 2009) with minor modifications: (1) All spines that protruded laterally from the dendritic shaft and exceeded a length of 0.4 μm were counted. (2) Spines that protruded into the z-plane were only counted if they exceeded the dendritic shaft more than 0.4 μm to the lateral side. (3) Spines that bisected were counted as two spines. (4) Spines had to be at least 10 μm away from branching points and the soma. Spine density was expressed as spines per μm of dendrite.

Prior to statistical analysis and blind to genotype, neurons were excluded if the image quality (poor signal to noise ratio) was not sufficient for counting of spines or for deconvolution.

Golgi staining

Golgi staining was done using the Rapid Golgi Staining Kit (FD NeuroTechnologies, USA) according to the manufacturer's instructions. All procedures were performed under dark conditions. One hemisphere of each mouse was used for Western blot analysis and the other hemisphere for Golgi staining (see Appendix Table S1 for sex of animals). Hemispheres were immersed in 2.5 ml mixtures of equal parts of kit solutions A and B and incubated at room temperature for 2 weeks. After 24 h solution A + B was renewed. Afterwards, brain tissues were stored in solution C at 4°C for at least 72 h, once exchanged after 24 h. Brains were snap-frozen on dry ice and coronal sections of 100 µm were cut with a cryotome (Hyrax C50, Zeiss, Germany). Each section was mounted with Solution C on an adhesive microscope slide pre-coated with 1% gelatin/0.1% chrome alum on both sides and stained according to the manufacturer's protocol with the exception that RotiClear (Roth, Germany) was used instead of xylene. Finally, slices were cover-slipped with Permount (Thermo Fisher Scientific, USA).

Imaging and analysis of spine density after Golgi staining

Imaging of second- or third-order dendritic branches of hippocampal pyramidal neurons of area CA1 was done with an Axio Observer Z1 (Zeiss, Germany) for Golgi-stained neurons using a 63x oil objective. Z-stack thickness was held constant at 130 nm. The number of spines was determined per micrometer of dendritic length (in total 100 µm per neuron) at apical and basal compartments using Neurolucida software (MicroBrightField, USA). Spines in the area around branching points and the soma were excluded from analysis. Five animals per genotype and 3-4 neurons per animal were analysed blind to genotype and injected viral vector.

Behavioral analysis

Animals

Mice (cDKO + AAV-APPsα: 9M + 9F, cDKO + AAV-Venus: 8M + 10F, LM control + AAV-Venus: 12M + 10F) were housed under a 12/12h light-dark cycle (lights on at 20:00) in groups of 2-5, unless individual housing was required by experimental protocols or to prevent fighting. Testing occurred during the dark phase under dim light (approximately 12 lux). Mice were transferred to the testing room 30 min before testing. Procedures were approved by the Veterinary Office of the Canton of Zurich (license 44/2015).

Behavioral procedures

Morris Water Maze place navigation. The round white poly-propylene pool had a diameter of 150 cm with 68 cm high walls. It was filled with water (24-26° C, depth 15 cm), rendered opaque by addition of 1 l of milk (UHT whole milk 3.5% fat, Coop, Switzerland). The white quadratic goal platform (14x14 cm) was made of metallic wire mesh. It was hidden 0.5 cm below the water surface in the center of one of the 4 quadrants, 30 cm from the side wall. Salient extra-maze cues were placed on the walls of the testing room. Animals performed 30 training trials (max. duration 120 s), 6 per day with intertrial intervals of 30-60 min and varying starting positions. During the first 18 trials the hidden platform was held in the same position (acquisition phase) and then moved to the opposite quadrant for the remaining 12 trials (reversal phase). The first 60 s of the first reversal trial served as probe trial to test for spatial retention. Time spent in a circular target zone comprising 12.5% of the pool surface was compared with corresponding control zones in adjacent quadrants.

Data analysis and statistics

The path of moving mice was tracked using Noldus EthoVision 3.1 (Noldus, Netherlands). For analysis all data were imported in custom programmed software Wintrack (www.wintrack.ch; Wolfer et al, 2001). Data were evaluated using an ANOVA model with genotype (cDKO + AAV-APPs α , cDKO + AAV-Venus, LM control + AAV-Venus) and sex as between subject factors. Within subject factors were added as needed to explore the dependence of genotype effects on place or time. Significant interactions and where necessary significant main effects were further explored by pairwise t-tests or by splitting the ANOVA model, as appropriate. Variables with strongly skewed distributions or strong correlations between variances and group means were subjected to Box-Cox transformation before statistical analysis. The significance threshold was set at 0.05. The false discovery rate (FDR) control procedure of Hochberg was applied to groups of conceptually related variables within single tests to correct significance thresholds for multiple comparisons. Similarly, FDR correction was applied during *post-hoc* testing. As genotype and treatment effects were independent of sex, the sex factor is not reported in results and figures. Statistical analyses were run using R version 3.2.3 complemented with the packages psych and moments.

For further methods related to EV Figures see Appendix Supplementary Methods

Results

AAV-APPs α injection mediates efficient and neuron specific expression of APPs α in the hippocampus of cDKO mice

To investigate whether APPs α is able to rescue the synaptic deficits of NexCre cDKO (further referred to as cDKO) animals *in vivo*, APPs α was expressed in the adult brain using stereotactic injection. We employed an AAV9-based bicistronic vector (AAV-APPs α ; Figure 1A) coding for Venus and codon-optimized HA-tagged murine HA-APPs α that was inserted behind the APP signal peptide (SP). The HA-APPs α reading frame was fused to Venus by a T2A site to enable tracking of transduced cells. Expression was driven by the neuronal synapsin promoter. Monocistronic AAV-Venus vector served as a control (AAV-Venus; Figure 1A). Adult cDKO animals (aged 4-5 months) were either injected with AAV-APPs α or AAV-Venus control vector, whereas littermate control mice (LM control) received only AAV-Venus. Thus, comparison of AAV-Venus injected cDKO mice with AAV-Venus injected LM controls was expected to yield similar synaptic impairments as previously observed for uninjected cDKO mice (Hick et al, 2015). Vectors were bilaterally injected (dose: 1.0×10^9 gc/ μ l per injection spot) into the stratum lacunosum moleculare region of the dorsal hippocampus and into the dentate gyrus (Figure 1B). To evaluate Venus and APPs α expression, animals were sacrificed 6 weeks post-injection and brain samples were analysed by Western blotting and immunohistochemistry using an HA-tag-specific antibody. Analysis of serial anteroposterior coronal brain sections (Bregma -1.10 to Bregma -2.70; see Figure EV1C) revealed widespread expression of APPs α in the hippocampus and, to a considerably lower extent, also in adjacent cortical areas (Figure 1C and EV1C). Along the longitudinal (dorsal-ventral) axis of the hippocampus APPs α expression was much more pronounced in the dorsal region, whereas expression was not detectable in the ventral hippocampus (Figure EV1C).

As Venus contained a membrane anchor, we observed prominent accumulation in dendritic regions, whereas HA-APPs α staining was intense in intracellular membrane compartments consistent with the transport of APPs α within the secretory pathway to the cell surface for secretion (see also Figure EV2D and E for co-localization with ER and Golgi markers). In the CA3 region APPs α expression appeared slightly lower compared to the expression obtained in pyramidal cells of the subiculum, the CA1 (Figure 1C) and the CA2 regions. Consistent with previous studies (Jackson et al, 2016), we noted that APPs α was detectable in HEK cells transfected with synapsin promoter driven AAV constructs (see Figure EV2A), likely due to AAV plasmid overload. *In vivo*, however, AAV-APPs α expression was restricted to neurons, as shown by double immunofluorescence staining against the HA-tag and the neuronal marker NeuN (Figure 1D and E). Consistently, no overlapping expression pattern was detectable in astrocytes (GFAP; Figure 1F) and microglia (Iba1; Figure 1G). The AAV-Venus expression pattern obtained from injections of control vector was largely similar to that

of AAV-APPs α (Figure EV1C). Western blot analysis of hippocampal homogenates, using the M3.2 antibody, confirmed efficient AAV-mediated APPs α expression in injected animals (Figure 1H). Note that antibody M3.2 is directed against an epitope located between the α - and β -secretase site and recognizes endogenous APP species (APP full length and APPs α) that are still expressed by interneurons and glia in cDKO mice (see Hick et al, 2015) and vector-derived AAV-APPs α . Collectively, our data demonstrate that AAV-APPs α injection results in efficient and neuron specific expression of APPs α throughout the dorsal hippocampus.

Impaired synaptic plasticity and reduced spine density of APP/APLP2 cDKO mice are rescued by APPs α expression in the adult brain

Having demonstrated that HA-APPs α is efficiently expressed in the hippocampus of injected animals we evaluated whether APPs α is sufficient to rescue impairments in functional network activity that were previously reported for cDKO mice (Hick et al, 2015). After 20 min of baseline recording we induced long-term potentiation (LTP) at the Schaffer collateral to CA1 pathway by application of theta burst stimulation (TBS) in acute hippocampal slices of mice that had been injected with viral vectors 6 weeks earlier (at 4-5 months of age). Consistent with our previous results (Hick et al, 2015) AAV-Venus injected cDKO mice exhibited significantly lower induction and maintenance of LTP (n=25 slices), as compared to AAV-Venus injected LM controls (n=23; Figure 2A). AAV-Venus injected LM control mice showed a potentiation of $156.69 \pm 4.75\%$ (t75-t80 after start of baseline recording) that was significantly reduced to only $128.12 \pm 3.41\%$ in AAV-Venus injected cDKO mice (one-way ANOVA followed by Bonferroni's *post-hoc* test, $^{###}p < 0.001$; Figure 2B). In contrast, the LTP curve recorded from acute slices of AAV-APPs α injected cDKO mice (n=24) closely overlapped with that of AAV-Venus injected LM controls (Figure 2A). Quantification of the last five minutes of recording revealed that APPs α rescued LTP deficits of cDKO mice to a level statistically indistinguishable from that of Venus injected LM controls (t75–80: $150.34 \pm 3.55\%$, $^{ns}p > 0.05$; Figure 2B). While basal synaptic transmission was comparable in all groups (see Figure EV3A and B), presynaptic function evaluated by paired pulse facilitation (PPF; Figure 2C) was significantly impaired in AAV-Venus injected cDKO mice at the 10 ms ($^{#}p < 0.05$) and 20 ms ($^{#}p < 0.05$) inter-stimulus intervals (ISI) in comparison to AAV-Venus injected LM controls. Strikingly, AAV-APPs α treatment lead to a highly significant rescue of short-term synaptic plasticity in cDKO mice as evidenced by PPF values statistically indistinguishable from LM controls (Figure 2C).

Next, we evaluated spine density as a correlate of excitatory synapses. To visualize neuronal morphology and spine density we performed iontophoretic postfixation filling with a

fluorescent dye of hippocampal CA1 pyramidal cells in brain slices from injected adult mice (aged 5-6 months). Consistent with our previous study (Hick et al, 2015), we confirmed a prominent reduction in spine density both in basal (100.00 ± 3.41 vs. 88.77 ± 3.10 spines/ μm , $\#p < 0.05$) and in midapical dendrites (100.00 ± 3.57 vs. 82.08 ± 4.73 spines/ μm , $\#p < 0.05$) of AAV-Venus injected cDKO CA1 neurons as compared to AAV-Venus injected LM controls (Figure 2D-F). In contrast, spine density of AAV-APPs α injected cDKO mice did not significantly differ from that of AAV-Venus injected LM control neurons, indicating that APPs α expression fully restored spine density in CA1 neurons. Collectively, these data demonstrate that acute expression of APPs α in adult mice is sufficient to rescue morphological and functional synaptic deficits in cDKO animals.

APPs α ameliorates dendritic branching abnormalities of cDKO animals

Prompted by the effect of APPs α on spine density we further evaluated its influence on the overall morphology and complexity of hippocampal CA1 neurons (Figure 3). In view of their different morphology and connectivity, basal and apical dendrites of CA1 neurons were studied separately. Neurons of AAV-Venus injected cDKO mice showed a significantly reduced total dendritic length and branching (as assessed by the number of nodes) in both basal and apical dendrites compared to AAV-Venus injected LM controls (Figure 3A-F). Impairments were readily apparent when visually inspecting reconstructed images of individual neurons (Figure 3A).

Although, total dendritic length was not significantly increased by APPs α expression in cDKO animals, the total number of nodes was significantly increased in basal dendrites of neurons from AAV-APPs α injected cDKO mice (Figure 3D) compared to injected LM controls (one-way ANOVA followed by Bonferroni's *post-hoc* test, $*p < 0.05$). To investigate whether changes in dendritic complexity may be more pronounced in distinct dendritic subregions we performed morphometric Sholl analysis. We plotted the dendritic length measured within circles centered on the soma against the distance from the cell body (see scheme in Figure 3B). In this analysis an increase in dendritic length per sphere corresponds to an increased dendritic complexity. Comparison of dendritic complexity between pyramidal neurons from AAV-Venus injected cDKO and LM control mice revealed an overall reduced dendritic complexity in cDKO neurons, both in basal (Figure 3G) and apical dendrites (Figure 3H). Branching deficits of basal dendrites from Venus injected cDKO neurons were most pronounced in proximal dendritic segments (60-90 μm from the soma). In apical dendrites both proximal regions (60-180 μm) and midapical regions (300 μm , 330 μm) were less complex. Interestingly, neurons of AAV-APPs α injected cDKO mice exhibited an intermediate curve with partially restored dendritic complexity. Sholl analysis revealed significantly increased dendritic complexity in proximal regions (60 μm) of basal dendrites of AAV-APPs α

injected cDKO neurons (repeated measures ANOVA followed by Sidaks's *post-hoc* test, $*p<0.05$; Figure 3G). Likewise, in apical dendrites of cDKO mice injected with AAV-APPs α , dendritic length was significantly increased at a distance of 300 μm ($**p<0.01$) and 330 μm ($**p<0.01$) as compared to neurons of AAV-Venus injected LM controls. Together, these data indicate that APPs α ameliorates branching deficits of cDKO mice at distinct dendritic regions.

APPs α improves spatial learning and spatial memory in cDKO mice

To evaluate whether improved synaptic density and plasticity is also reflected at the behavioural level we assessed spatial learning and memory in the Morris water maze (MWM) place navigation task (Figure 4). To this end, cDKO mice were either injected with AAV-Venus (n=18, red circles) or with AAV-APPs α (n=18, green circles) at 4-5 months of age and tested 2 months later at 6-7 months of age. For comparison, LM controls were injected with AAV-Venus (n=22, white circles). While swim speed was comparable in all groups (Figure 4A), we observed an overall impaired performance in AAV-Venus injected cDKO mice both during acquisition and reversal training. Although all three groups of mice did show learning, escape latencies (Figure 4B) and swim path lengths (Figure 4C) were significantly increased in Venus injected cDKO mice compared to Venus injected LM controls, especially at day 2 and 3 of acquisition, learning and for the last trials of reversal learning. These data are highly consistent with and confirm the deficit in spatial learning observed previously in uninjected cDKO mice (Hick et al, 2015). Overall, APPs α expression in cDKO mice lead to an intermediate performance with significantly improved learning during the reversal phase. AAV-APPs α expression in cDKO mice significantly decreased escape latency ($**p<0.01$; Figure 4B) and swim path length ($*p<0.05$; Figure 4C) at day 5 of reversal learning, as compared to AAV-Venus injected cDKO mice. During the probe trial that assesses spatial reference memory, analysis of time [%] spend in the target zone (Figure 4D) reveals a significant overall group x place effect ($F(2, 46)=9.095$, $p=0.0005$). AAV-Venus injected cDKO mice were strongly impaired in comparison to AAV-Venus injected controls ($###p<0.001$) and failed to prefer the trained target zone. Time spend in the target zone was not significantly different from chance level. Strikingly, AAV-APPs α expression substantially improved probe trial performance in cDKO mice compared to Venus injected cDKO mice ($**p<0.01$). Moreover, AAV-APPs α injected cDKOs showed a highly significant preference for the trained target zone over adjacent quadrants ($**p<0.01$). Together these data indicate that expression of APPs α in the adult hippocampus substantially improved spatial reference memory.

APPs β does not rescue LTP or spine density *in vivo*

During AD BACE expression is upregulated (Ahmed et al, 2010; Holsinger et al, 2002) leading to increased amyloidogenic APP processing and thus increased APPs β levels. Although APPs β has been reported to be less potent in assays of neuroprotection *in vitro* (Barger & Harmon, 1997; Copanaki et al, 2010; Furukawa et al, 1996), the molecular basis of this property has remained elusive and its *in vivo* role is currently unknown. We therefore evaluated in a separate set of experiments whether APPs β , being only 16 amino acids shorter compared to APPs α (see Figure 5B) might also be able to rescue the impairments of cDKO mice. Briefly, we stereotactically injected cDKO mice and LM controls (4-5 months of age) with AAV-Venus or a bicistronic vector coding for Venus and HA-tagged murine APPs β (AAV-APPs β ; Figure 5A). Immunohistochemistry of serial brain sections indicated that injection of AAV-APPs β yielded a comparable expression level and distribution to that obtained for HA-APPs α (Figure 5C and EV1C). Western blot analysis of total hippocampal homogenates (containing cell bound and secreted proteins), using an HA-tag specific antibody further confirmed similar (and statistically not significantly different) levels of HA-APPs β and HA-APPs α expression upon injection of the respective AAVs (unpaired two-tailed Student's t test, ^{ns} $p>0.05$; Figure 5D and E). Ultracentrifugation (UC) of the same hippocampal homogenates was used to specifically detect soluble HA-APPs α and HA-APPs β (Figure 5D, lower boxed panels) and yielded comparable levels of APPs α and APPs β in UC supernatants (unpaired two-tailed Student's t test, ^{ns} $p>0.05$; Figure 5D and E). Transfection of HEK cells (Figure EV2A) with the APPs α or APPs β encoding AAV plasmids or transduction of cultured neurons with either of the AAV vectors (Figure EV2B), further confirmed efficient and comparable secretion of APPs α or APPs β , as evidenced by Western blot analysis of cell supernatants (Figure EV2A and B).

Strikingly, despite comparable levels of expression and secretion, soluble APPs β failed to exert any detectable effects on basal synaptic transmission (Figure EV3C and D) or synaptic plasticity in recordings of cDKO slices at 5-6 months of age (Figure 5F-H). AAV-APPs β injected cDKO mice showed superimposable LTP curves compared to Venus injected cDKO mice. Potentiation at t75-80 min after start of baseline recording was not significantly different (cDKO + AAV-Venus: $125.58 \pm 2.69\%$ vs. cDKO + AAV-APPs β : $124.42 \pm 1.96\%$, ^{ns} $p>0.05$, unpaired two-tailed Students t-test). Moreover, also in the PPF paradigm AAV-APPs β expression did not lead to any detectable difference compared to AAV-Venus control injections (Figure 5H). Likewise, and consistent with electrophysiological analysis, AAV-APPs β failed to rescue spine density deficits of cDKO mice determined upon Golgi staining. While AAV-Venus control-injected cDKO revealed again a significant reduction in spine density in basal and in apical dendrites as compared to Venus injected LM controls (Figure 5 I-K), spine density was comparable and statistically indistinguishable in AAV-Venus and

APPs β injected cDKO mice. Basal dendrites from AAV-Venus and AAV-APPs β injected cDKO mice showed a similar and statistically not significantly different reduction in spine density of 14% (LM control + Venus: 100 ± 2.84 vs. cDKO + APPs β : 85.99 ± 3.51 spines/ μm , * $p < 0.05$) and 12% (LM control + Venus: 100 ± 2.84 vs. cDKO + APPs β : 88.39 ± 3.26 spines/ μm , **** $p < 0.0001$), respectively (Figure 5J). In midapical dendritic segments spine density was reduced by 24% in AAV-Venus injected cDKO animals (LM control + Venus: 100 ± 4.01 vs. cDKO + APPs β : 76.05 ± 2.097 spines/ μm) or by 18% (LM control + Venus: 100 ± 4.01 vs. cDKO + APPs β : 82.40 ± 3.28 spines/ μm) in AAV-APPs β injected animals, respectively (Figure 5K). Together, these data indicate a striking difference in the *in vivo* properties of secreted APPs, with APPs α ameliorating morphological and functional synaptic deficits of cDKO mice, while APPs β had no effect.

APPs α facilitates LTP via its C-terminal CT α 16 domain

Prompted by these results, we now focused on the 16 amino acids domain (CT α 16) that distinguishes APPs α from APPs β (Figure 5B and L-Q). Previously, we had demonstrated that a short incubation of slices with recombinant APPs α (recAPPs α) is sufficient to largely rescue the LTP deficits of cDKO mice (Hick et al, 2015). To determine whether this acute function of APPs α is mediated by the CT α 16 domain, we now pre-incubated cDKO slices for 60 min at room temperature either with a synthetic CT α 16 peptide (10 nM), or with CT α 16_{scr} (10 nM), a scrambled peptide of the same aminoacid composition. After 20 min of baseline recording LTP was again induced by TBS. During the whole measurement, the peptides diluted in ACSF were circulating in a closed-loop system. Strikingly, we found that the application of CT α 16 potently facilitated LTP over the whole recording period (Figure 5L and M) including the early phase of post tetanic potentiation (t20-25, CT α 16: $191.49 \pm 8.82\%$ vs. CT α 16_{scr}: $165.12 \pm 8.82\%$, * $p < 0.01$; Figure 5L and M) and led to a highly significant increase in LTP values 60 min after the beginning of baseline recording (t75-80, CT α 16: $148.08 \pm 3.65\%$ vs. CT α 16_{scr}: $132.18 \pm 4.26\%$, ** $p < 0.01$; Figure 5L and M). In contrast, LTP values obtained for CT α 16_{scr} were very similar to those after AAV-Venus injection into cDKO mice (t75-80, $128.12 \pm 3.41\%$; Figure 2B). CT α 16 peptide application also significantly improved and restored PPF of cDKO slices (Figure 5N) to values comparable to that obtained for AAV-Venus injected LM control mice (see Figure 2C). Next, we directly compared the activity of CT α 16 and recAPPs α (Figure 5O-Q) that was purified from stably transfected HEK cell supernatants. We found that CT α 16 application (10 nM) was as potent as recAPPs α (10 nM) in rescuing both the LTP (t75-80, APPs α : $146.15 \pm 4.21\%$ vs. CT α 16: $148.08 \pm 3.65\%$, ^{ns} $p > 0.05$) and PPF deficit of cDKO slices. Values obtained were statistically indistinguishable (Figure 5O and P). Together, these data identify the CT α 16 domain of APPs α as sufficient to mediate the functions of APPs α for enhancing synaptic plasticity *in vitro*.

Inhibition of $\alpha 7$ -nAChR by BTX blocks APPs α mediated effects on LTP

While elevated (micromolar) A β concentrations and aggregated A β species exert an inhibitory effect on synaptic function (Gu & Yakel, 2011; Kamenetz et al, 2003; Shankar et al, 2007) picomolar concentrations of soluble A β have previously been demonstrated to enhance LTP and PTP in a mechanism dependent on the activity of $\alpha 7$ nicotinic acetylcholine receptors ($\alpha 7$ -nAChRs; Puzzo et al, 2011; Puzzo et al, 2008). As the CT $\alpha 16$ domain of APPs α overlaps with the N-terminus of A β we therefore tested whether signalling by $\alpha 7$ -nAChR may mediate the LTP facilitating functions of APPs α . First, we hypothesized that if $\alpha 7$ -nAChRs are crucially involved in the LTP facilitating effect of APPs α , pharmacological block of $\alpha 7$ -nAChR should impair LTP in LM control mice that still express APP and APPs α . Indeed, treatment of slices with 10 nM α -bungarotoxin (α -BTX), a specific inhibitor of $\alpha 7$ -nAChRs significantly reduced LTP during the induction phase (t20-25, LM control: $184.01 \pm 5.59\%$ vs. LM control + BTX: $158.04 \pm 8.35\%$, * $p < 0.05$) and the maintenance phase (t75-80, LM control: $147.25 \pm 3.87\%$ vs. LM control + BTX: $131.24 \pm 4.99\%$, * $p < 0.05$; Figure 6A and B). Values obtained after BTX treatment were very similar to those of CT $\alpha 16_{scr}$ treated cDKO slices (compare to Figure 5L and M, CT $\alpha 16_{scr}$ treated cDKO slices: $132.18 \pm 4.26\%$).

Next, we tested how α -BTX affects the induction of LTP by exogenous application of recAPPs α or CT $\alpha 16$ (Figures 6,C-G and EV4). When α -BTX was added after the incubation of slices with either recAPPs α or CT $\alpha 16$ 30 min before TBS (Figure EV4A, scheme) we observed only a small but not significant reduction in LTP (Figure EV4B-E). In contrast, if α -BTX was co-applied together with recAPPs α for 1 h before TBS (Figure 6C, scheme), this lead to a significant inhibition as compared to recAPPs α treatment alone (Figure 6D and E) both during the LTP induction phase (t20-25, recAPPs α : $168.49 \pm 7.20\%$ vs. recAPPs α + BTX: $142.57 \pm 7.75\%$, * $p < 0.05$; Figure 6D and E) and the LTP maintenance phase (t75-80, recAPPs α : $135.59 \pm 3.81\%$ vs recAPPs α + BTX: $118.58 \pm 5.51\%$, * $p < 0.05$; Figure 6D and E). Similarly, if α -BTX was co-applied together with the CT $\alpha 16$ peptide for 1 h before TBS (Figure 6F and G) this lead to a significant inhibition as compared to CT $\alpha 16$ treatment alone both during the LTP induction phase (t20-25, CT $\alpha 16$: $176.23 \pm 4.69\%$ vs. CT $\alpha 16$ + BTX: $153.75 \pm 5.05\%$, * $p < 0.05$; Figure 6F and G) and the LTP maintenance phase (t75-80, CT $\alpha 16$: $144.37 \pm 2.34\%$ vs CT $\alpha 16$ + BTX: $129.24 \pm 3.40\%$, ** $p < 0.01$; Figure 6F and G). Together, these data suggest that APPs α exerts its functions on LTP mainly via the CT $\alpha 16$ domain in a mechanism depending on $\alpha 7$ -nAChR function. Further studies are needed to address whether improvements in spine density and behavior that we observed upon AAV-APPs α re-expression might also depend on $\alpha 7$ -nAChR function.

APPs α shows high-affinity allosteric potentiation of $\alpha 7$ -nAChR expressed in *Xenopus* oocytes

To investigate whether CT $\alpha 16$ can modulate $\alpha 7$ -nAChRs directly, homomeric $\alpha 7$ -nAChRs were expressed in *Xenopus laevis* oocytes, and nicotine- or acetylcholine-induced currents at submaximal EC₅₀ agonist concentration (100 μ M) were measured either alone or after pre-application of CT $\alpha 16$ by two-electrode voltage clamp. Upon application of 100 nM of CT $\alpha 16$ alone, no activation of $\alpha 7$ -nAChRs was detectable (data not shown). Remarkably, 100 nM of CT $\alpha 16$ significantly potentiated both, nicotine- and acetylcholine-induced currents with a 2.58 ± 0.42 -fold ($n=8$) and 3.01 ± 0.96 -fold ($n=7$) enhancement of $\alpha 7$ -nAChRs responses, respectively (paired two-tailed Students t-test, $*p<0.05$; Figure 7A and B). In contrast, no significant effect of 100 nM CT $\alpha 16_{scr}$ on nicotine-induced currents could be detected (1.00 ± 0.06 -fold increase, paired two-tailed Students t-test, $n=5$; $^{ns}p>0.05$; Figure 7A and B). Dose-response analysis of CT $\alpha 16$ concentrations between 1 and 100 nM yielded an EC₅₀ value for CT $\alpha 16$ of 10.7 ± 4.6 nM with an hill-coefficient of 2.1 ± 0.3 for $\alpha 7$ -nAChRs ($n=4$; Figure 7C). To establish if the physiological APPs α fragment that contains the CT $\alpha 16$ sequence at the C-terminus can also modulate $\alpha 7$ -nAChRs, we tested the effect of 20 nM recAPPs α , a concentration close to the 10 nM that facilitated LTP in slices, on nicotine-gated currents (Figure 7D-F). Indeed, 20 nM recAPPs α significantly potentiated nicotine-induced currents (3.35 ± 0.81 -fold enhancement, paired two-tailed Students t-test, $n=4$; $*p<0.05$) to a similar extent as seen with 100 nM of CT $\alpha 16$ (Figure 7D and E, see Figure 7A for comparison). This effect could be specifically blocked by BTX (Figure 7D). Notably, and consistent with experiments in slices, no significant potentiation was seen upon pre-application of 20 nM recAPPs β (1.32 ± 0.18 -fold enhancement, paired two-tailed Students t-test, $n=5$, $^{ns}p>0.05$; Figure 7D and E). As a further control, we investigated whether APPs α may also modulate other pentameric ion channels. However, neither recAPPs α nor CT $\alpha 16$ had any effects on the structurally related homomeric $\alpha 1$ -GlyR (Figure EV5), indicating that APPs α specifically acts on $\alpha 7$ -nAChRs. Next, to gain further mechanistic insight, we analyzed nicotine dose-responses of $\alpha 7$ -nAChRs in the presence of a potentiating concentration of recAPPs α to see how APPs α modulates $\alpha 7$ -nAChRs (Figure 7F). Strikingly, 20 nM recAPPs α shifted the nicotine dose-response curve to the left and lead to an approximately 2-fold significant decrease in the EC₅₀ of nicotine (40.3 ± 6.0 μ M) as compared to recAPPs α -free conditions (EC₅₀ of 80.5 ± 12.7 μ M, paired two-tailed Students t-test, $n=5$, $*p<0.05$) without affecting the hill-coefficient (3.3 ± 0.5 vs. 3.7 ± 0.9 , paired two-tailed Students t-test, $^{ns}p>0.05$) and the maximal inducible nicotine currents (Figure 7F). Together, these data indicate that APPs α

acts as a potent (nanomolar range) positive allosteric modulator of $\alpha 7$ -nAChRs by increasing the apparent agonist affinity.

Discussion

In this study we provide compelling evidence for distinct functional roles of the two secreted APP ectodomain fragments APPs α and APPs β *in vivo* and provide functional insight into the underlying mechanism. Long-term AAV mediated expression of either APPs α or APPs β in the hippocampus of adult NexCre cDKO (cDKO) mice revealed several important new findings: (1) *In vivo* expression of APPs α efficiently rescued deficits in spine density, synaptic plasticity (LTP and PPF) and spatial reference memory of cDKO mice. (2) In contrast to APPs α , APPs β expression had no detectable effects on spine density and synaptic plasticity in cDKO mice indicating distinct functional roles in the adult CNS. (3) The C-terminal 16 amino acids (CT α 16) of APPs α proved sufficient to enhance LTP to the same extent as full length APPs α . (4) Nanomolar concentrations of APPs α and CT α 16 function as potent positive allosteric modulators of $\alpha 7$ -nAChRs *in vitro* increasing the apparent agonist affinity. (5) Pharmacological blockade of $\alpha 7$ -nAChRs impaired the APPs α (or CT α 16) induced LTP facilitation, thus identifying $\alpha 7$ -nAChRs as physiological APPs α receptors that are involved to mediate its LTP enhancing effects.

Our previous studies indicated that LTP deficits of cDKO mice can be rescued by acute application of nanomolar amounts of APPs α , but not APPs β , *in vitro*. Despite this, it remained unclear whether these acute *in vitro* effects observed for a short time of recording would also be relevant *in vivo* and whether reduced spine density and behavioural deficits might also be rescued. Lastly, the mechanism by which APPs α regulates LTP including the relevant receptor was unknown. In principle, synaptic deficits of cDKO mice may either arise from developmental deficits such as impaired synaptogenesis that could lead to miswired circuits or may be due to a lack of APP (or APLP2) mediated functions in the adult brain. To address these questions and to assess the specific role(s) of the secreted ectodomains APPs α and APPs β we used a reverse genetic approach employing AAV mediated re-expression of APPs α or APPs β in the hippocampus of adult cDKO mice. Expression of the AAV-Venus control vector in cDKO mice or littermate controls fully reproduced and confirmed the phenotype of cDKO mice (Hick et al, 2015) including reduced dendritic complexity (Figure 3) and spine density of CA1 neurons (Figure 2), deficits in synaptic plasticity (Figure 2), as well as impaired spatial memory (Figure 4). This indicates that the cDKO phenotype is robust and that AAV vectors are suitable to confer neuron-specific, long lasting and widespread expression throughout the dorsal hippocampus (see Figure 1 and EV1). Using this *in vivo* reconstitution approach we show that APPs α is not only able to acutely modulate synaptic

strength when applied *in vitro* (Hick et al, 2015), but has the ability to mediate a long-lasting rescue of synaptic plasticity, with facilitating effects on both the induction and maintenance phase of LTP. Moreover, we show that APPs α re-expression rescued spine density, a correlate of excitatory synapses. These data are perfectly in line with our recent observation that a lack of APP and thus APPs α in APP-KO mice leads to impairments in structural spine plasticity in the cortex (Zou et al, 2016). While synaptic plasticity and spine density were completely restored, APPs α expression led only to a partial rescue of dendritic complexity of CA1 neurons with effects most pronounced close to the soma and in the midapical region of apical dendrites. These more subtle effects might in part be related to a potential non-uniform secretion of APPs α along dendritic regions of individual neurons that may become limiting at more distant regions. Alternatively, it is conceivable that APPs α is not sufficient to fully restore neurite outgrowth and dendritic arbours due to an inability to compensate early developmental defects or an additional requirement for APLP2 (Hick et al, 2015; Weyer et al, 2014). In this regard neither deficiency of APP nor APLP2 alone results in reduced dendritic complexity in young adult knockout mice (Lee et al, 2010; Midthune et al, 2012; Tyan et al, 2012) while a combined absence in cDKO mice profoundly impairs neuronal morphology and total neurite length (Hick et al, 2015; Weyer et al, 2014 and this study) indicating a combined role of APP and APLP2 for dendritic complexity. Although the underlying mechanism is still unknown, it appears likely that domains conserved between APP and APLP2 (and not divergent sequences as those close to the secretase sites) are involved.

The ability of synapses to undergo long-term potentiation is considered as a cellular mechanism underlying learning and memory (reviewed by Korte & Schmitz, 2016). Indeed, restoration of LTP by APPs α at the CA3/CA1 pathway was associated with a significantly improved performance in water maze place navigation during reversal learning (Figure 4B and C) and a substantial increase of spatial reference memory, as assessed during the probe trial. In mice, emotional reactions to the swim stress are a limiting factor for performance during task acquisition, that becomes less relevant during reversal learning as mice get habituated to the stressful experience (Lipp & Wolfer, 1998; Strange et al, 2014). The dorsal hippocampus known to mediate spatial processing (Strange et al, 2014) was efficiently targeted by AAV-APPs α injections whereas AAV-APPs α was undetectable in ventral portions of the hippocampus (Figure EV1C) that mediate emotional responses. Thus, a failure to compensate emotional problems due to selective targeting may explain why AAV-APPs α treatment effects were only seen during probe trial and reversal learning. Although hippocampal lesions have been demonstrated to impair hippocampus dependent behaviour (Morris et al, 1982), learning and memory also involves other brain regions that were not targeted by the injections including the dorsomedial striatum – prefrontal cortex network

which is strongly involved in the initial acquisition of the place-navigation task (Woolley et al, 2013). The entorhinal cortex constitutes a crucial interface between the hippocampus and the rest of the cortex and is the source of most spatial information that is processed in the hippocampus (Hales et al, 2014; Vorhees & Williams, 2014). The fact that AAV-APP α expression was largely restricted to the hippocampus may thus underlie the partial but not complete rescue of performance by APP α in the MWM. In addition, part of the behavioural deficits may also be due to developmental effects of the mutation.

Consistent with an important function of APP α in the mature brain, acute depletion of APP α in wild type animals by either pharmacological inhibition of α -secretase (Taylor et al, 2008), or infusion of antibodies directed against the C-terminus of APP α (Puzzo et al, 2011; Taylor et al, 2008) was reported to impair LTP and cognitive behaviour. However, these previous approaches lacked specificity, as secretase inhibitors target also other substrates besides APP and antibodies employed bind not only to APP α , but also full length APP and A β . Collectively, our findings indicate an important synaptotrophic role of APP α in the mature CNS for spine density, synaptic plasticity and behaviour. Importantly, this role in cDKO mice (lacking endogenous APP and all its fragments including A β) is completely independent of any indirect A β related effects, in contrast to the previously reported A β lowering properties of APP α in transgenic APP/PS1 mice (Fol et al, 2016; Obregon et al, 2012).

As APP α and APP β are identical in primary sequence except for the last 16 amino acids one may expect that they should exhibit largely overlapping functions. Accordingly, only few studies have so far directly compared the effects mediated by either APP α or APP β . *In vitro*, recombinant APP β was shown to more efficiently induce the differentiation of human embryonic stem cells into neuronal precursor cells as compared to APP α (Freude et al, 2011), whereas a similar increase in axonal outgrowth was observed when cortical neurons were treated with recombinant APP β or APP α (Chasseigneaux et al, 2011). With regard to *in vitro* assays of neuroprotection, however, APP β was considerably less potent to protect neurons against glucose deprivation, excitotoxicity, A β peptide (Barger & Harmon, 1997; Furukawa et al, 1996) or epoxomicin induced proteasomal stress (Copanaki et al, 2010). Here, we compared the *in vivo* functions of the secreted APP ectodomains in the adult brain. A surprising key finding was that APP α and APP β exert strikingly different effects *in vivo*, despite a similar level and pattern of AAV mediated expression (Figure 1, 5C-E, EV1 and EV2). Of note, the absence of beneficial effects by AAV-APP β cannot be simply explained by possible adverse effects associated with AAV-APP β expression, as we found no signs of increased cell death, nor any evidence for increased astrogliosis or microgliosis (see

Appendix Figure S1) as unspecific signs of neurodegeneration. Although earlier studies had indicated that a fragment (N-APPs1-286) derived for APPs β may induce caspase activation and death of sensory neurons in a mechanism requiring DR6 (Nikolaev et al, 2009), these data have recently been revised to exclude a requirement for β -secretase activity and thus APPs β (Olsen et al, 2014). Our notion that AAV-APPs β does not induce adverse effects is further in agreement with previous data from fully viable and apparently normal APPs β -knockin (KI) mice expressing solely APPs β (Li et al, 2010). However, whether a lack of APPs α in APPs β -KI mice might lead to synaptic deficits, had remained unknown.

We demonstrate that APPs α but not APPs β rescues spine density and synaptic plasticity in cDKO mice and identified the CT α 16 peptide of APPs α as a crucial LTP-enhancing functional domain that stimulated LTP to the same extent as recAPPs α . Mechanistically, facilitation of LTP by APPs α or the CT α 16 peptide required functional α 7-nAChRs since BTX, a selective antagonist of α 7-nAChRs, blocked its effects. Moreover, when expressed in oocytes α 7-nAChRs could be directly potentiated by nanomolar amounts of either recAPPs α (but not recAPPs β) or CT α 16 in the presence of ACh or nicotine. Together with the ability of APPs α to enhance the sensitivity of α 7-nAChRs for the agonist nicotine these data establish APPs α as a potent positive allosteric modulator (PAM). These findings also suggests that APPs α might function as an endogenous PAM of cholinergic signalling in the hippocampus, although further studies are required to confirm its activity *in vivo*. Several studies have shown that nAChR activation facilitates LTP induction (for review see Yakel, 2014) and α 7-nAChRs are abundantly expressed in the hippocampus (Fabian-Fine et al, 2001). Several mechanisms of α 7-nAChR signalling are thought to contribute to its role in LTP: (1) activation of presynaptic α 7-nAChR can increase glutamate release and (2) activation of postsynaptic α 7-nAChRs that have a high Ca²⁺ permeability may confer membrane depolarisation and induce plasticity evoking Ca²⁺ signalling (reviewed by McKay et al, 2007; Yakel, 2014).

Although more work is needed to understand precisely how APPs α affects α 7-nAChR signalling, we hypothesize that both pre- and postsynaptic mechanisms are likely to play a role. When applied to slices of cDKO mice both APPs α and CT α 16 enhanced, in a BTX sensitive manner, the early phase of post tetanic potentiation (PTP) during the first minutes after start of baseline recording, which is believed to involve Ca²⁺ build up in presynaptic terminals. In line with an important endogenous role of APPs α for LTP, APPs α secretion is activity dependent (Fazeli et al, 1994; Gakhar-Koppole et al, 2008; Hoey et al, 2009; Mills & Reiner, 1999) and can thus be increased through plasticity-inducing protocols. The enhancement of PTP by APPs α , as observed in our study, is consistent with previous studies that reported increased Ca²⁺ influx in synaptoneurosomes and α 7-nAChRs transfected

neuroblastoma cells upon application of low (picomolar) amounts of A β or N-terminal A β -peptides that are overlapping with the C-terminus of APPs α (Dougherty et al, 2003; Lawrence et al, 2014). Recently, low (picomolar) amounts of A β were shown to increase synaptic vesicle recycling via α 7-nAChRs signalling in hippocampal neurons (Lazarevic et al, 2017). Moreover, low amounts of A β had been found to stimulate synaptic plasticity and memory in wildtype mice (Lawrence et al, 2014; Puzzo et al, 2011). In addition to presynaptic effects it is likely that APPs α will also modulate signalling at the postsynaptic site (for a review see Ludewig & Korte, 2016). Postsynaptic membrane depolarization due to Ca²⁺ influx through α 7-nAChRs may increase the probability of NMDAR-activation that is crucial to induce stable LTP. In this regard, NMDAR inhibition has been shown to prevent the nicotine induced conversion of short term plasticity into LTP at CA3/CA1 synapses (Ji et al, 2001). Moreover, also activation of septal cholinergic input to induce α 7-nAChRs dependent LTP required the activation of NMDARs (Gu & Yakel, 2011). In addition to signalling via α 7-nAChRs, APPs α may also modulate NMDARs more directly, as APPs α was shown to potentiate tetanically evoked NMDAR currents recorded at granule cells of the dentate gyrus in rat brain slices (Taylor et al, 2008) and full length APP can biochemically interact with GluN1/GluN2 receptors (Cousins et al, 2009), although it is not known whether this also holds true for APPs α .

Our finding of distinct *in vivo* functions of APPs α and APPs β have important implications for AD therapy. Pharmacological BACE1 inhibition has been a major approach to reduce A β in animals and clinical trials. More recently, however, concerns have been raised that therapeutic BACE1 inhibition may also compromise important physiological functions of BACE (Yan & Vassar, 2014). Indeed, BACE-KO mice display deficits in synaptic morphology and synaptic plasticity in the hippocampus (Dominguez et al, 2005; Laird et al, 2005). Our data indicate that APPs β deficiency that will result from BACE1 inhibition is unlikely to lead to toxic effects. A number of recent studies demonstrated that very low concentrations of A β may stimulate transmitter release and modulate synaptic plasticity and memory. Strikingly, we now show that it is the C-terminal domain of APPs α that is required to increase spine density, rescues LTP and improves memory. As this C-terminal domain is also present in A β it is conceivable that signaling of APPs α and soluble, non-aggregated A β species may at least in part converge e.g. regarding the activation of α 7-nAChRs. From this, one may speculate that APPs α may be able to rescue potential unwanted effects due to limited A β levels. It is also clear however, that sequence context and structural accessibility of the CT α 16 domain is crucial. Indeed, the presence of the CT α 16 domain appears to alter the conformation of APPs α in a critical way. Analysis by small angle X-ray diffraction indicated that the 3D structure of APPs α and APPs β are quite different, with APPs α exhibiting an extended conformation with an exposed CT α 16 region (Gralle et al, 2006; Peters-Libeu et al,

2015) while in APPs β the E1 domain folds back towards the C-terminal juxtamembrane region (Peters-Libeu et al, 2015). Thus, different 3D structures may enable or prevent binding to receptors, which may contribute to the distinct *in vivo* functions of APPs α and APPs β .

Regarding AD pathogenesis our data indicate that a shift towards β -secretase processing that may occur during AD (Ahmed et al, 2010; Holsinger et al, 2002) could result in insufficient amounts of APPs α that cannot be functionally compensated by APPs β . A lack or reduction of APPs α might thus contribute to deficits in synaptic plasticity and cognitive function in AD patients. Consistent with this notion, in AD patients hippocampal levels of synaptically localized ADAM10/SAP97 complexes are reduced (Epis et al, 2010) and an activity attenuating mutation in the human ADAM10 gene leading to reduced APPs α levels has been associated with AD (Kim et al, 2009; Suh et al, 2013). In familial AD cases carrying the Swedish mutation (APP_{SWE}), cerebrospinal fluid (CSF) levels of APPs α were found to be reduced already at early stages of AD (Almkvist et al, 1997; Lannfelt et al, 1995). With regard to sporadic AD cases, however, no consensus has been reached whether reduced APPs α levels are associated with AD (Mockett et al, 2017). Early on, total soluble APPs was reported to be severely reduced in sporadic AD (Van Nostrand et al, 1992). Several more recent studies specifically detecting APPs α reported reduced APPs α levels in mild (Sennvik et al, 2000) to moderate AD (Rosen et al, 2012), or in APOE4 positive AD patients (Olsson et al, 2003), while several other studies found no difference in APPs α at early stages of sporadic AD (Brinkmalm et al, 2013; Perneczky et al, 2013; Perneczky et al, 2011; Rosen et al, 2012). These mixed results may in part be related to different assays systems used and the recent finding of considerable diurnal variability of APPs α and other APP fragments in the CSF (Dobrowolska et al, 2014). Thus, more detailed studies are needed to resolve these important issues.

In preclinical AD research, numerous studies have been conducted using APP transgenic mouse models (<https://www.alzforum.org/research-models>) which (over)express huAPP_{SWE} that undergoes enhanced β -secretase processing. Consequently, reduced levels of neuroprotective and synaptotrophic APPs α relative to increased amounts of A β (that is a reduced APPs α /A β ratio) may fail to adequately balance and antagonize the detrimental effects of A β and thus contribute to the phenotypic and synaptic impairments in these transgenic mice.

APPs α also plays an important role in processes of natural aging. Not only is memory performance correlated with APPs α levels in rats (Anderson et al, 1999), but also aging-

related deficits in LTP and cognitive behaviour can be rescued by exogenous APPs α (Moreno et al, 2015; Xiong et al, 2016). Collectively, our findings indicate distinct functions for APPs α in the adult brain to modulate spine density, synaptic plasticity and cognition. Our findings lend further support to therapeutic approaches aimed at directly or indirectly increasing APPs α expression in the brain (Mockett et al., 2017, Müller et al, 2017) to ameliorate synaptic deficits in AD or possibly also for other diseases in which neurons are damaged.

Author contributions

UCM designed and conceived the study. MCR, SK and SW performed intracranial AAV injections and analyzed data. CB and KH produced recombinant APPs. MCR performed and analyzed experiments related to APPs expression analysis in vitro and in vivo including Western blots, performed immunochemistry and Sholl analysis including spine density measurements. SL, LRS and MK performed extracellular electrophysiological recordings in brain slices, analyzed data and interpreted results. AW and BL performed electrophysiological recordings in oocytes, analyzed data and interpreted results. TA and CJB generated AAV vectors and analyzed APPs expression in neurons. AKF and DPW conducted, analyzed and interpreted behavioral experiments. UCM wrote the manuscript with help from MCR and input from all authors.

Acknowledgements

We acknowledge funding by the Deutsche Forschungsgemeinschaft (grant FOR1332 to MK and UM, MU1457/14-1 to UM) and by the Else-Kröner Fresenius-Stiftung (2014-A229 to UM). DPW is a member of the of the Neuroscience Center Zurich (ZNZ) and of the Zurich Center for Integrative Human Physiology (ZIHP). We thank Annette Nicke for providing the plasmid encoding the $\alpha 7$ -nAChR cDNA.

References

Ahmed RR, Holler CJ, Webb RL, Li F, Beckett TL, Murphy MP (2010) BACE1 and BACE2 enzymatic activities in Alzheimer's disease. *J Neurochem* **112**: 1045-1053

Almkvist O, Basun H, Wagner SL, Rowe BA, Wahlund LO, Lannfelt L (1997) Cerebrospinal fluid levels of alpha-secretase-cleaved soluble amyloid precursor protein mirror cognition in a Swedish family with Alzheimer disease and a gene mutation. *Arch Neurol* **54**: 641-644

Anderson JJ, Holtz G, Baskin PP, Wang R, Mazzarelli L, Wagner SL, Menzaghi F (1999) Reduced cerebrospinal fluid levels of alpha-secretase-cleaved amyloid precursor protein in aged rats: correlation with spatial memory deficits. *Neuroscience* **93**: 1409-1420

Barger SW, Harmon AD (1997) Microglial activation by Alzheimer amyloid precursor protein and modulation by apolipoprotein E. *Nature* **388**: 878-881

Brinkmalm G, Brinkmalm A, Bourgeois P, Persson R, Hansson O, Portelius E, Mercken M, Andreasson U, Parent S, Lipari F, Ohrfelt A, Bjerke M, Minthon L, Zetterberg H, Blennow K, Nutu M (2013) Soluble amyloid precursor protein alpha and beta in CSF in Alzheimer's disease. *Brain Res* **1513**: 117-126

Chasseigneaux S, Allinquant B (2012) Functions of Abeta, sAPPalpha and sAPPbeta : similarities and differences. *J Neurochem* **120 Suppl 1**: 99-108

Chasseigneaux S, Dinc L, Rose C, Chabret C, Couplier F, Topilko P, Mauger G, Allinquant B (2011) Secreted amyloid precursor protein beta and secreted amyloid precursor protein alpha induce axon outgrowth in vitro through Egr1 signaling pathway. *PLoS One* **6**: e16301

Copanaki E, Chang S, Vlachos A, Tschape JA, Muller UC, Kogel D, Deller T (2010) sAPPalpha antagonizes dendritic degeneration and neuron death triggered by proteasomal stress. *Mol Cell Neurosci* **44**: 386-393

Cousins SL, Hoey SE, Anne Stephenson F, Perkinson MS (2009) Amyloid precursor protein 695 associates with assembled NR2A- and NR2B-containing NMDA receptors to result in the enhancement of their cell surface delivery. *J Neurochem* **111**: 1501-1513

D'Costa S, Blouin V, Broucque F, Penaud-Budloo M, Francois A, Perez IC, Le Bec C, Moullier P, Snyder RO, Ayuso E (2016) Practical utilization of recombinant AAV vector reference standards: focus on vector genomes titration by free ITR qPCR. *Mol Ther Methods Clin Dev* **5**: 16019

Dawson GR, Seabrook GR, Zheng H, Smith DW, Graham S, O'Dowd G, Bowery BJ, Boyce S, Trumbauer ME, Chen HY, Van der Ploeg LH, Sirinathsinghji DJ (1999) Age-related cognitive deficits, impaired long-term potentiation and reduction in synaptic marker density in mice lacking the beta-amyloid precursor protein. *Neuroscience* **90**: 1-13

Dobrowolska JA, Kasten T, Huang Y, Benzinger TL, Sigurdson W, Ovod V, Morris JC, Bateman RJ (2014) Diurnal patterns of soluble amyloid precursor protein metabolites in the human central nervous system. *PLoS One* **9**: e89998

Dominguez D, Tournoy J, Hartmann D, Huth T, Cryns K, Deforce S, Serneels L, Camacho IE, Marjaux E, Craessaerts K, Roebroek AJ, Schwake M, D'Hooge R, Bach P, Kalinke U, Moechars D, Alzheimer C, Reiss K, Saftig P, De Strooper B (2005) Phenotypic and biochemical analyses of BACE1- and BACE2-deficient mice. *J Biol Chem* **280**: 30797-30806

Dougherty JJ, Wu J, Nichols RA (2003) Beta-amyloid regulation of presynaptic nicotinic receptors in rat hippocampus and neocortex. *J Neurosci* **23**: 6740-6747

Epis R, Marcello E, Gardoni F, Vastagh C, Malinverno M, Balducci C, Colombo A, Borroni B, Vara H, Dell'Agli M, Cattabeni F, Giustetto M, Borsello T, Forloni G, Padovani A, Di Luca M (2010) Blocking ADAM10 synaptic trafficking generates a model of sporadic Alzheimer's disease. *Brain* **133**: 3323-3335

Fabian-Fine R, Skehel P, Errington ML, Davies HA, Sher E, Stewart MG, Fine A (2001) Ultrastructural distribution of the alpha7 nicotinic acetylcholine receptor subunit in rat hippocampus. *J Neurosci* **21**: 7993-8003

Fazeli MS, Breen K, Errington ML, Bliss TV (1994) Increase in extracellular NCAM and amyloid precursor protein following induction of long-term potentiation in the dentate gyrus of anaesthetized rats. *Neurosci Lett* **169**: 77-80

Fol R, Braudeau J, Ludewig S, Abel T, Weyer SW, Roederer JP, Brod F, Audrain M, Bemelmans AP, Buchholz CJ, Korte M, Cartier N, Muller UC (2016) Viral gene transfer of APP α rescues synaptic failure in an Alzheimer's disease mouse model. *Acta neuropathologica* **131**: 247-266

Freude KK, Penjwini M, Davis JL, LaFerla FM, Blurton-Jones M (2011) Soluble amyloid precursor protein induces rapid neural differentiation of human embryonic stem cells. *J Biol Chem* **286**: 24264-24274

Furukawa K, Sopher BL, Rydel RE, Begley JG, Pham DG, Martin GM, Fox M, Mattson MP (1996) Increased activity-regulating and neuroprotective efficacy of alpha-secretase-derived secreted amyloid precursor protein conferred by a C-terminal heparin-binding domain. *J Neurochem* **67**: 1882-1896

Gakhar-Koppole N, Hundeshagen P, Mandl C, Weyer SW, Allinquant B, Muller U, Ciccolini F (2008) Activity requires soluble amyloid precursor protein alpha to promote neurite outgrowth in neural stem cell-derived neurons via activation of the MAPK pathway. *Eur J Neurosci* **28**: 871-882

Gralle M, Oliveira CL, Guerreiro LH, McKinsty WJ, Galatis D, Masters CL, Cappai R, Parker MW, Ramos CH, Torriani I, Ferreira ST (2006) Solution conformation and heparin-induced dimerization of the full-length extracellular domain of the human amyloid precursor protein. *J Mol Biol* **357**: 493-508

Gu Z, Yakel JL (2011) Timing-dependent septal cholinergic induction of dynamic hippocampal synaptic plasticity. *Neuron* **71**: 155-165

Hales JB, Schlesiger MI, Leutgeb JK, Squire LR, Leutgeb S, Clark RE (2014) Medial entorhinal cortex lesions only partially disrupt hippocampal place cells and hippocampus-dependent place memory. *Cell reports* **9**: 893-901

Heber S, Herms J, Gajic V, Hainfellner J, Aguzzi A, Rulicke T, von Kretschmar H, von Koch C, Sisodia S, Tremml P, Lipp HP, Wolfer DP, Muller U (2000) Mice with combined gene knock-outs reveal essential and partially redundant functions of amyloid precursor protein family members. *J Neurosci* **20**: 7951-7963

Hefter D, Kaiser M, Weyer SW, Papageorgiou IE, Both M, Kann O, Muller UC, Draguhn A (2016) Amyloid Precursor Protein Protects Neuronal Network Function after Hypoxia via Control of Voltage-Gated Calcium Channels. *J Neurosci* **36**: 8356-8371

Hick M, Herrmann U, Weyer SW, Mallm JP, Tschape JA, Borgers M, Mercken M, Roth FC, Draguhn A, Slomianka L, Wolfer DP, Korte M, Muller UC (2015) Acute function of secreted amyloid precursor protein fragment APPsalpha in synaptic plasticity. *Acta neuropathologica* **129**: 21-37

Hoey SE, Williams RJ, Perkinson MS (2009) Synaptic NMDA receptor activation stimulates alpha-secretase amyloid precursor protein processing and inhibits amyloid-beta production. *J Neurosci* **29**: 4442-4460

Holsinger RM, McLean CA, Beyreuther K, Masters CL, Evin G (2002) Increased expression of the amyloid precursor beta-secretase in Alzheimer's disease. *Ann Neurol* **51**: 783-786

Holtmaat A, Bonhoeffer T, Chow DK, Chuckowree J, De Paola V, Hofer SB, Hubener M, Keck T, Knott G, Lee WC, Mostany R, Mrsic-Flogel TD, Nedivi E, Portera-Cailliau C, Svoboda K, Trachtenberg JT, Wilbrecht L (2009) Long-term, high-resolution imaging in the mouse neocortex through a chronic cranial window. *Nat Protoc* **4**: 1128-1144

Jackson KL, Dayton RD, Deverman BE, Klein RL (2016) Better Targeting, Better Efficiency for Wide-Scale Neuronal Transduction with the Synapsin Promoter and AAV-PHP.B. *Front Mol Neurosci* **9**: 116

Ji D, Lape R, Dani JA (2001) Timing and location of nicotinic activity enhances or depresses hippocampal synaptic plasticity. *Neuron* **31**: 131-141

Kamenetz F, Tomita T, Hsieh H, Seabrook G, Borchelt D, Iwatsubo T, Sisodia S, Malinow R (2003) APP processing and synaptic function. *Neuron* **37**: 925-937

Kendel Y, Melaun C, Kurz A, Nicke A, Peigneur S, Tytgat J, Wunder C, Mebs D, Kaufenstein S (2013) Venomous secretions from marine snails of the Terebridae family target acetylcholine receptors. *Toxins (Basel)* **5**: 1043-1050

Kim M, Suh J, Romano D, Truong MH, Mullin K, Hooli B, Norton D, Tesco G, Elliott K, Wagner SL, Moir RD, Becker KD, Tanzi RE (2009) Potential late-onset Alzheimer's disease-associated mutations in the ADAM10 gene attenuate {alpha}-secretase activity. *Human molecular genetics* **18**: 3987-3996

Klevanski M, Saar M, Baumkotter F, Weyer SW, Kins S, Muller UC (2014) Differential role of APP and APLPs for neuromuscular synaptic morphology and function. *Mol Cell Neurosci* **61C**: 201-210

Korte M, Schmitz D (2016) Cellular and System Biology of Memory: Timing, Molecules, and Beyond. *Physiol Rev* **96**: 647-693

Laird FM, Cai H, Savonenko AV, Farah MH, He K, Melnikova T, Wen H, Chiang HC, Xu G, Koliatsos VE, Borchelt DR, Price DL, Lee HK, Wong PC (2005) BACE1, a major determinant of selective vulnerability of the brain to amyloid-beta amyloidogenesis, is essential for cognitive, emotional, and synaptic functions. *J Neurosci* **25**: 11693-11709

Lannfelt L, Basun H, Wahlund LO, Rowe BA, Wagner SL (1995) Decreased alpha-secretase-cleaved amyloid precursor protein as a diagnostic marker for Alzheimer's disease. *Nat Med* **1**: 829-832

Laube B, Hirai H, Sturgess M, Betz H, Kuhse J (1997) Molecular determinants of agonist discrimination by NMDA receptor subunits: analysis of the glutamate binding site on the NR2B subunit. *Neuron* **18**: 493-503

Laube B, Kuhse J, Betz H (1998) Evidence for a tetrameric structure of recombinant NMDA receptors. *J Neurosci* **18**: 2954-2961

Laube B, Kuhse J, Betz H (2000) Kinetic and mutational analysis of Zn(2+) modulation of recombinant human inhibitory glycine receptors. *The Journal of Physiology* **522**: 215-230

Lawrence JL, Tong M, Alfulaij N, Sherrin T, Contarino M, White MM, Bellinger FP, Todorovic C, Nichols RA (2014) Regulation of presynaptic Ca²⁺, synaptic plasticity and contextual fear conditioning by a N-terminal beta-amyloid fragment. *J Neurosci* **34**: 14210-14218

Lazarevic V, Fienko S, Andres-Alonso M, Anni D, Ivanova D, Montenegro-Venegas C, Gundelfinger ED, Cousin MA, Fejtova A (2017) Physiological Concentrations of Amyloid Beta Regulate Recycling of Synaptic Vesicles via Alpha7 Acetylcholine Receptor and CDK5/Calcineurin Signaling. *Front Mol Neurosci* **10**: 221

Lee KJ, Moussa CE, Lee Y, Sung Y, Howell BW, Turner RS, Pak DT, Hoe HS (2010) Beta amyloid-independent role of amyloid precursor protein in generation and maintenance of dendritic spines. *Neuroscience* **169**: 344-356

Li H, Wang B, Wang Z, Guo Q, Tabuchi K, Hammer RE, Sudhof TC, Zheng H (2010) Soluble amyloid precursor protein (APP) regulates transthyretin and Klotho gene expression without rescuing the essential function of APP. *Proc Natl Acad Sci U S A* **107**: 17362-17367

Lipp HP, Wolfer DP (1998) Genetically modified mice and cognition. *Curr Opin Neurobiol* **8**: 272-280

Ludewig S, Korte M (2016) Novel Insights into the Physiological Function of the APP (Gene) Family and Its Proteolytic Fragments in Synaptic Plasticity. *Front Mol Neurosci* **9**: 161

McKay BE, Placzek AN, Dani JA (2007) Regulation of synaptic transmission and plasticity by neuronal nicotinic acetylcholine receptors. *Biochem Pharmacol* **74**: 1120-1133

Meziane H, Dodart JC, Mathis C, Little S, Clemens J, Paul SM, Ungerer A (1998) Memory-enhancing effects of secreted forms of the beta-amyloid precursor protein in normal and amnesic mice. *Proc Natl Acad Sci U S A* **95**: 12683-12688

Midthune B, Tyan SH, Walsh JJ, Sarsoza F, Eggert S, Hof PR, Dickstein DL, Koo EH (2012) Deletion of the amyloid precursor-like protein 2 (APLP2) does not affect hippocampal neuron morphology or function. *Mol Cell Neurosci* **49**: 448-455

Mills J, Reiner PB (1999) Mitogen-activated protein kinase is involved in N-methyl-D-aspartate receptor regulation of amyloid precursor protein cleavage. *Neuroscience* **94**: 1333-1338

Milosch N, Tanriover G, Kundu A, Rami A, Francois JC, Baumkötter F, Weyer SW, Samanta A, Jaschke A, Brod F, Buchholz CJ, Kins S, Behl C, Müller UC, Kogel D (2014) Holo-APP and G-protein-mediated signaling are required for sAPP α -induced activation of the Akt survival pathway. *Cell death & disease* **5**: e1391

Mockett BG, Richter M, Abraham WC, Müller UC (2017) Therapeutic Potential of Secreted Amyloid Precursor Protein APP α . *Front Mol Neurosci* **10**: 30

Moreno L, Rose C, Mohanraj A, Allinquant B, Billard JM, Dutar P (2015) sA β APP α Improves Hippocampal NMDA-Dependent Functional Alterations Linked to Healthy Aging. *J Alzheimers Dis* **48**: 927-935

Morris RG, Garrud P, Rawlins JN, O'Keefe J (1982) Place navigation impaired in rats with hippocampal lesions. *Nature* **297**: 681-683

Müller UC, Deller T, Korte M (2017) Not just amyloid: physiological functions of the amyloid precursor protein family. *Nat Rev Neurosci* **18**: 281-298

Nikolaev A, McLaughlin T, O'Leary DD, Tessier-Lavigne M (2009) APP binds DR6 to trigger axon pruning and neuron death via distinct caspases. *Nature* **457**: 981-989

Obregon D, Hou H, Deng J, Giunta B, Tian J, Darlington D, Shahaduzzaman M, Zhu Y, Mori T, Mattson MP, Tan J (2012) Soluble amyloid precursor protein- α modulates beta-secretase activity and amyloid- β generation. *Nat Commun* **3**: 777

Olsen O, Kallop DY, McLaughlin T, Huntwork-Rodriguez S, Wu Z, Duggan CD, Simon DJ, Lu Y, Easley-Neal C, Takeda K, Hass PE, Jaworski A, O'Leary DD, Weimer RM, Tessier-Lavigne M (2014) Genetic analysis reveals that amyloid precursor protein and death receptor 6 function in the same pathway to control axonal pruning independent of beta-secretase. *J Neurosci* **34**: 6438-6447

Olsson A, Hoglund K, Sjögren M, Andreasen N, Minthon L, Lannfelt L, Buerger K, Möller HJ, Hampel H, Davidsson P, Blennow K (2003) Measurement of α - and β -secretase cleaved amyloid precursor protein in cerebrospinal fluid from Alzheimer patients. *Exp Neurol* **183**: 74-80

Pernecky R, Guo LH, Kagerbauer SM, Werle L, Kurz A, Martin J, Alexopoulos P (2013) Soluble amyloid precursor protein β as blood-based biomarker of Alzheimer's disease. *Translational psychiatry* **3**: e227

Perneckzy R, Tsolakidou A, Arnold A, Diehl-Schmid J, Grimmer T, Forstl H, Kurz A, Alexopoulos P (2011) CSF soluble amyloid precursor proteins in the diagnosis of incipient Alzheimer disease. *Neurology* **77**: 35-38

Peters-Libeu C, Campagna J, Mitsumori M, Poksay KS, Spilman P, Sabogal A, Bredesen DE, John V (2015) sAbetaPPalpha is a Potent Endogenous Inhibitor of BACE1. *J Alzheimers Dis* **47**: 545-555

Plummer S, Van den Heuvel C, Thornton E, Corrigan F, Cappai R (2016) The Neuroprotective Properties of the Amyloid Precursor Protein Following Traumatic Brain Injury. *Aging Dis* **7**: 163-179

Puzzo D, Privitera L, Fa M, Staniszewski A, Hashimoto G, Aziz F, Sakurai M, Ribe EM, Troy CM, Mercken M, Jung SS, Palmeri A, Arancio O (2011) Endogenous amyloid-beta is necessary for hippocampal synaptic plasticity and memory. *Ann Neurol* **69**: 819-830

Puzzo D, Privitera L, Leznik E, Fa M, Staniszewski A, Palmeri A, Arancio O (2008) Picomolar amyloid-beta positively modulates synaptic plasticity and memory in hippocampus. *J Neurosci* **28**: 14537-14545

Ring S, Weyer SW, Kilian SB, Waldron E, Pietrzik CU, Filippov MA, Herms J, Buchholz C, Eckman CB, Korte M, Wolfer DP, Muller UC (2007) The secreted beta-amyloid precursor protein ectodomain APPs alpha is sufficient to rescue the anatomical, behavioral, and electrophysiological abnormalities of APP-deficient mice. *J Neurosci* **27**: 7817-7826

Rosen C, Andreasson U, Mattsson N, Marcusson J, Minthon L, Andreasen N, Blennow K, Zetterberg H (2012) Cerebrospinal fluid profiles of amyloid beta-related biomarkers in Alzheimer's disease. *Neuromolecular medicine* **14**: 65-73

Saftig P, Lichtenthaler SF (2015) The alpha secretase ADAM10: A metalloprotease with multiple functions in the brain. *Prog Neurobiol* **135**: 1-20

Seabrook GR, Smith DW, Bowery BJ, Easter A, Reynolds T, Fitzjohn SM, Morton RA, Zheng H, Dawson GR, Sirinathsinghji DJ, Davies CH, Collingridge GL, Hill RG (1999) Mechanisms contributing to the deficits in hippocampal synaptic plasticity in mice lacking amyloid precursor protein. *Neuropharmacology* **38**: 349-359

Selkoe DJ, Hardy J (2016) The amyloid hypothesis of Alzheimer's disease at 25 years. *EMBO Mol Med* **8**: 595-608

Sennvik K, Fastbom J, Blomberg M, Wahlund LO, Winblad B, Benedikz E (2000) Levels of alpha- and beta-secretase cleaved amyloid precursor protein in the cerebrospinal fluid of Alzheimer's disease patients. *Neurosci Lett* **278**: 169-172

Shankar GM, Bloodgood BL, Townsend M, Walsh DM, Selkoe DJ, Sabatini BL (2007) Natural oligomers of the Alzheimer amyloid-beta protein induce reversible synapse loss by modulating an NMDA-type glutamate receptor-dependent signaling pathway. *J Neurosci* **27**: 2866-2875

Strange BA, Witter MP, Lein ES, Moser EI (2014) Functional organization of the hippocampal longitudinal axis. *Nat Rev Neurosci* **15**: 655-669

Suh J, Choi SH, Romano DM, Gannon MA, Lesinski AN, Kim DY, Tanzi RE (2013) ADAM10 missense mutations potentiate beta-amyloid accumulation by impairing prodomain chaperone function. *Neuron* **80**: 385-401

Taylor CJ, Ireland DR, Ballagh I, Bourne K, Marechal NM, Turner PR, Bilkey DK, Tate WP, Abraham WC (2008) Endogenous secreted amyloid precursor protein-alpha regulates hippocampal NMDA receptor function, long-term potentiation and spatial memory. *Neurobiol Dis* **31**: 250-260

Tyan SH, Shih AY, Walsh JJ, Maruyama H, Sarsoza F, Ku L, Eggert S, Hof PR, Koo EH, Dickstein DL (2012) Amyloid precursor protein (APP) regulates synaptic structure and function. *Mol Cell Neurosci* **51**: 43-52

Van Nostrand WE, Wagner SL, Shankle WR, Farrow JS, Dick M, Rozemuller JM, Kuiper MA, Wolters EC, Zimmerman J, Cotman CW, Cunningham DD (1992) Decreased levels of soluble amyloid beta-protein precursor in cerebrospinal fluid of live Alzheimer disease patients. *Proc Natl Acad Sci U S A* **89**: 2551-2555

Vassar R, Kuhn PH, Haass C, Kennedy ME, Rajendran L, Wong PC, Lichtenthaler SF (2014) Function, therapeutic potential and cell biology of BACE proteases: current status and future prospects. *J Neurochem* **130**: 4-28

von Koch CS, Zheng H, Chen H, Trumbauer M, Thinakaran G, van der Ploeg LH, Price DL, Sisodia SS (1997) Generation of APLP2 KO mice and early postnatal lethality in APLP2/APP double KO mice. *Neurobiol Aging* **18**: 661-669

Vorhees CV, Williams MT (2014) Assessing spatial learning and memory in rodents. *ILAR J* **55**: 310-332

Wang P, Yang G, Mosier DR, Chang P, Zaidi T, Gong YD, Zhao NM, Dominguez B, Lee KF, Gan WB, Zheng H (2005) Defective neuromuscular synapses in mice lacking amyloid precursor protein (APP) and APP-Like protein 2. *J Neurosci* **25**: 1219-1225

Weyer SW, Klevanski M, Delekate A, Voikar V, Aydin D, Hick M, Filippov M, Drost N, Schaller KL, Saar M, Vogt MA, Gass P, Samanta A, Jaschke A, Korte M, Wolfer DP, Caldwell JH, Muller UC (2011) APP and APLP2 are essential at PNS and CNS synapses for transmission, spatial learning and LTP. *EMBO J* **30**: 2266-2280

Weyer SW, Zagrebelsky M, Herrmann U, Hick M, Ganss L, Gobbert J, Gruber M, Altmann C, Korte M, Deller T, Muller UC (2014) Comparative analysis of single and combined APP/APLP knockouts reveals reduced spine density in APP-KO mice that is prevented by APP α expression. *Acta neuropathologica communications* **2**: 36

Wolfer DP, Madani R, Valenti P, Lipp HP (2001) Extended analysis of path data from mutant mice using the public domain software Wintrack. *Physiol Behav* **73**: 745-753

Woolley DG, Laeremans A, Gantois I, Mantini D, Vermaercke B, Op de Beeck HP, Swinnen SP, Wenderoth N, Arckens L, D'Hooze R (2013) Homologous involvement of striatum and prefrontal cortex in rodent and human water maze learning. *Proc Natl Acad Sci U S A* **110**: 3131-3136

Xiong M, Jones OD, Peppercorn K, Ohline SM, Tate WP, Abraham WC (2016) Secreted amyloid precursor protein- α can restore novel object location memory and hippocampal LTP in aged rats. *Neurobiol Learn Mem*

Yakel JL (2014) Nicotinic ACh receptors in the hippocampal circuit; functional expression and role in synaptic plasticity. *J Physiol* **592**: 4147-4153

Yan R, Vassar R (2014) Targeting the beta secretase BACE1 for Alzheimer's disease therapy. *Lancet Neurol* **13**: 319-329

Zou C, Crux S, Marinesco S, Montagna E, Sgobio C, Shi Y, Shi S, Zhu K, Dorostkar MM, Muller UC, Herms J (2016) Amyloid precursor protein maintains constitutive and adaptive plasticity of dendritic spines in adult brain by regulating D-serine homeostasis. *EMBO J* **35**

Figure Legends

Figure 1: Expression of APP α in the hippocampus of AAV-APP α injected cDKO animals. **A** Schematic representation of monocistronic and bicistronic AAV constructs enabling neuron-specific expression of i) Venus and ii) HA-tagged APP α (+ Venus). ITR: inverted terminal repeat, Synapsin: promotor, T2A: *Thoseaasigna* virus 2A site, SP: signal peptide, HA: influenza hemagglutinin tag. **B** Scheme of the hippocampus with coordinates of the two injection sites (black stars). **C** Overview of the hippocampus of an AAV-APP α injected cDKO mouse. HA-tag staining (red) reveals APP α expression within the CA1, CA3 and DG of the hippocampus. Magnification shows the boxed CA1 region. Scale bars: 500 μ m (left), 100 μ m (right). DG: Dentate Gyrus, CA: Cornus Ammonis. **D-G** Double immunostaining in CA1 region. APP α (HA-tag, red) is exclusively expressed in neurons (NeuN, blue, **D, E**), but not in astrocytes (GFAP, blue, **F**) or microglia (Iba1, blue, **G**). Scale bars: 10 μ m (**D, F, G**), 5 μ m (**E**). **H** Western blot analysis of APP expression in hippocampus of LM control (N=5) and cDKO mice (N=5) injected with AAV-Venus or AAV-APP α . Age of mice: 5-6 months.

Figure 2: AAV-APPs α rescues LTP, impaired short-term synaptic plasticity and spine density of cDKO mice. **A, B** LTP was induced at hippocampal CA3-CA1 synapses after 20 min baseline recordings (arrowhead, TBS). cDKO mice expressing Venus (red) exhibited significant lower induction and maintenance of LTP ($128.12 \pm 3.41\%$) compared to Venus injected LM controls (white, $156.69 \pm 4.75\%$, $^{###}p < 0.001$). AAV mediated expression of APPs α (green) restored potentiation after start of baseline recording and resulted in an LTP curve comparable to that of LM controls. The LTP induction rate is shown as percentage % of mean baseline slope. Data points were averaged over 6 time points. **C** The deficit of PPF in Venus injected cDKO mice at the 10 ms ($^{#}p < 0.05$) and 20 ms ($^{#}p < 0.05$) ISI was restored by expression of APPs α . n=number of slices. N=number of animals. **D** Representative images of basal and midapical dendritic segments of CA1 neurons. **E, F** The spine density deficit of Venus injected cDKOs mice (11% in basal and 18% in midapical dendrites) is rescued by APPs α to LM control levels. Images are maximum projections of deconvolved z-stacks. Scale bar: 5 μ m. Spine density was normalized to LM control levels. n=number of neurons (from 5 animals per condition). **A-F** Age of mice at analysis: 5-6 months. Data represent mean \pm SEM. Data were analyzed by one-way ANOVA followed by Bonferroni's *post-hoc* test. # indicates significant differences between LM control and cDKO injected with AAV-Venus, * between cDKO injected with AAV-Venus or APPs α . $^{ns}p > 0.05$, $^{*/#}p < 0.05$, $^{**/##}p < 0.01$, $^{***/###}p < 0.001$.

Figure 3: APPs α ameliorates dendritic branching abnormalities of cDKO animals

A Representative 3D-reconstructions of CA1 pyramidal neurons from AAV-Venus injected LM controls (left), AAV-Venus injected cDKOs (middle, red) and AAV-APPs α injected cDKOs (right, green). **B** Schematic representation of parameters assessed. **C-F** Compared to LM controls AAV-Venus injected cDKO mice show a significantly reduced basal ($^{##}p < 0.01$, **C**) and apical ($^{##}p < 0.01$, **E**) dendritic length and reduced branching in basal ($^{##}p < 0.01$, **D**) and apical ($^{##}p < 0.01$, **F**) dendrites. AAV-APPs α injection did neither affect basal ($^{ns}p > 0.05$, **C**) nor apical ($^{ns}p > 0.05$, **E**) total dendritic length. However, the total number of basal nodes differed significantly compared to AAV-Venus injected cDKO mice ($^{*}p < 0.05$, **D**). **G** Sholl analysis of basal dendritic length reveals a significant group effect (repeated measures ANOVA: genotype $F(2,$

29)=5.038, $p<0.05$) and a significant distance effect (repeated measures ANOVA: genotype $F(5, 145)=250.2$, $p<0.0001$). Due to a significant interaction effect (repeated measures ANOVA: genotype $F(10, 145)=4.466$, $p<0.0001$), a *post-hoc* Sidak's multiple comparison test was performed to further evaluate effects between groups at distinct distances from soma. Compared to Venus injection, AAV-APPs α injection of cDKO significantly increased basal dendritic length at 60 μm (* $p<0.05$). **H** Sholl analysis of apical dendritic length reveals an overall significant group effect (repeated measures ANOVA: genotype $F(2, 37)=4.776$, $p<0.05$) and a significant distance effect (repeated measures ANOVA: genotype $F(18, 666)=47.54$, $p<0.0001$). Due to a significant interaction effect (repeated measures ANOVA: genotype $F(36, 666)=1.640$, $p<0.05$), a *post-hoc* Sidak's multiple comparison test was performed to further evaluate effects between groups at distinct distances from soma. AAV-APPs α expression increased midapical dendritic length at 300 μm (** $p<0.01$) and 330 μm (** $p<0.01$) distance from soma compared to AAV-Venus injected cDKO mice. **A-H** Age of mice: 5-6 months. n =number of neurons (from 4-5 animals per condition). Data represent mean \pm SEM. Data were analyzed by one-way ANOVA followed by Bonferroni's *post-hoc* test (**C-F**) or repeated measures ANOVA followed by Bonferroni's or Sidak's *post-hoc* test (**G-H**). # indicates significant differences between LM control and cDKO injected with AAV-Venus, * between cDKO injected with AAV-Venus or APPs α , • between LM control injected with Venus and cDKO injected with AAV-APPs α . ^{ns} $p>0.05$, */#/* $p<0.05$, **/###/•• $p<0.01$, ***/###/••• $p<0.001$.

Figure 4: APPs α improves place navigation and spatial memory of cDKO mice in the MWM **A** Swim speed during acquisition and reversal learning is comparable in all groups (each point represents one day with 6 trials). **B** During acquisition learning and after platform reversal to the opposite quadrant, AAV-Venus injected cDKOs (red circles) show considerably longer escape latency compared to AAV-Venus injected LM controls (white circles). AAV-APPs α injected cDKO mice (green circles) show an overall intermediate performance (genotype $F(2, 46)=6.361$, $p=0.0036$) and that differs significantly at day 5 of reversal learning compared to AAV-Venus injected cDKO mice (genotype \times day $F(8, 184)=5.266$, $p<0.0001$; ** $p<0.01$). **C** Measurements of swim path length confirms the training performance deficit of cDKO mice compared to LM controls. During the reversal phase, the performance of AAV-APPs α injected cDKOs is significantly improved at day 5 (genotype $F(2, 46)=16.70$,

$p < 0.0001$, genotype \times day $F(8,184) = 5.788$, $p < 0.0001$; * $p < 0.05$, •• $p < 0.01$). **D** In the probe trial, AAV-Venus injected cDKOs (red) spend significantly less time in the target zone compared to AAV-Venus (### $p < 0.001$) injected LM control animals (white) and failed to prefer it significantly over control zones in adjacent quadrants. Note that expression of APPs α (green) largely rescues the deficits of cDKOs. N=22 (LM controls: AAV-Venus), N=18 (cDKOs: AAV-Venus), N=18 (cDKOs: AAV-APPs α). Data represent mean \pm SEM. Dashed lines: chance level. Data were analyzed using a mixed ANOVA model with conditions (LM control: AAV-Venus, cDKO: AAV-Venus and cDKO: AAV-APPs α) as between subject factor. Within subject factors were added to explore the dependence of genotype effects on day and place. Significant interactions and main effects were further explored by pairwise FDR-corrected two-tailed Student's t-tests. # indicates significant differences between LM control and cDKO injected with AAV-Venus, * between cDKO injected with AAV-Venus or APPs α , • between LM control injected with Venus and cDKO injected with AAV-APPs α . ^{ns} $p > 0.05$, */#• $p < 0.05$, **/###/•• $p < 0.01$, ***/###/••• $p < 0.001$.

Figure 5: AAV-APPs β fails to rescue LTP or spine density *in vivo*, while CT α 16 facilitates LTP *in vitro*. **A** Schematic representation of AAV9 constructs enabling the neuron-specific expression of i) Venus and ii) HA-tagged APPs β (+ Venus). ITR: inverted terminal repeat, Synapsin: neuron specific promotor, T2A: *Thoseaasigna* virus 2A site, SP: signal peptide, HA: influenza hemagglutinin tag. **B** APPs α differs from APPs β in the last 16 C-terminal amino acids (CT α 16, green). The epitope recognized by the M3.2 antibody is indicated. **C** Overview of the hippocampus of a AAV-APPs β (HA-tag, red) injected cDKO mouse. APPs β is expressed in CA1, CA3 and DG. Scale bar: 500 μ m. DG: dentate gyrus, CA: Cornus Ammonis. **D** Western blot analysis of HA-APPs α and HA-APPs β in hippocampi of injected mice (boxed upper panel), probed with an HA-tag specific antibody (lower band, arrowhead; *unspecific signal). Homogenates of AAV injected hippocampi were subjected to ultracentrifugation to detect soluble APPs α and APPs β (UC supernatant; boxed lower panel). The APP C-terminal antibody Y188 was used to confirm the separation of soluble APPs α from membrane bound full-length APP that is detected in total lysates of AAV-Venus injected littermate controls. Hippocampi of APP^{-/-} mice served as a negative control for antibody specificity. **E** Quantification of HA-APPs α and HA-APPs β expression in total hippocampal homogenates and of soluble HA-APPs after

UC normalized to β -tubulin. Note the comparable expression in AAV-APPs α and AAV-APPs β injected mice. Age: 5-6 months. N=Number of animals. Data represent mean \pm SEM. Data were analyzed by unpaired two-tailed Student's t test. ^{ns}p>0.05.

F-H Activity dependent synaptic plasticity was investigated in cDKO after injection of AAV-Venus (red) or APPs β (blue). **F, G** AAV-mediated overexpression of APPs β (n=23 slices, blue symbols) failed to rescue the LTP defect of cDKO mice (n=24 slices, red symbols). **G** TBS induced strengthening of fEPSPs resulted in similar potentiation levels for the last 5 minutes of recording (t75-80). The LTP induction rate is shown as percentage % of mean baseline slope. Data points were averaged over 6 time points. **H** PPF paradigm yielded no significant differences between viral vector injected cDKO mice. Age: 5-6 months. n=number of recorded slices. N=number of animals. Data represent mean \pm SEM. Data were analyzed unpaired two-tailed Students t-test. **I** Representative images of Golgi stained midapical and basal dendritic segments of LM control and cDKO animals injected with AAV-Venus or AAV-APPs β . **J, K** The significant spine density deficit of AAV-Venus injected cDKO mice (red bar) in basal (**J**) and apical dendrites (**K**) was comparable and not significantly different (^{ns}p>0.05) from that of AAV-APPs β injected cDKO mice (blue bar). White bar: AVV-Venus injected LM controls. Images are maximum projections of z-stacks. Scale bar: 5 μ m. Spine density is normalized to LM control levels. Age: 5-6 months; n=number of neurons (from 5 animals per condition). Data represent mean \pm SEM. Data were analyzed by one-way ANOVA followed by Bonferroni's *post-hoc* test. *p<0.05, **p<0.01, ***p<0.001, ****p<0.0001 . **L, M** Acute hippocampal slices of cDKO were pre-incubated for 1 hour either with 10 nM CT α 16 or CT α 16_{scr} before inducing LTP by TBS (arrowhead). Averaged potentiation levels at LTP induction (t20-25) revealed a significantly enhancement by CT α 16 as compared to CT α 16_{scr} present over the whole recoding time. Potentiation levels at t75-80 are significantly increased in the presence of CT α 16 (**p<0.01). The LTP induction rate is shown as percentage % of mean baseline slope. Data points were averaged over 6 time points. **N** CT α 16 significantly enhances short-term synaptic plasticity at inter-stimulus intervals of 40 (**p<0.01), 80 (*p<0.05), and 160 (**p<0.01) ms compared to CT α 16_{scr}. **O-Q** Acute application of CT α 16 and recAPPs α elevates LTP in cDKO slices to the same extent. **O, P** After 1 hour pre-incubation with either 10 nM CT α 16 or 10 nM recAPPs α fEPSPs were recorded. The TBS induced LTP curve was closely overlapping for both conditions and resulted in similar, statistically not significantly

different LTP values **Q** CT α 16 and recAPPs α modulate presynaptic function of cDKO mice in the same manner. Age: 5-6 months. n=number of recorded slices. N=number of animals. Data represent mean \pm SEM. Data were analyzed by unpaired two-tailed Students t-test.

Figure 6: LTP facilitation by APPs α or CT α 16 requires functional α 7-nAChRs

A, B Treatment with 10 nM α -BTX (30 min prior to TBS, black circles) significantly reduces LTP induction (t20-25, phase of post tetanic potentiation) and maintenance (t75-80) in LM controls expressing endogenous APP and APPs α . The LTP induction rate is shown as percentage % of mean baseline slope. Data points were averaged over 6 time points. **C** Experimental set-up: co-application of recAPPs α or CT α 16 and BTX before LTP induction. Peptides and BTX inhibitor used for pre-incubation circulated throughout the whole LTP recording. **D, E** Co-application of BTX and recAPPs α significantly inhibits synaptic plasticity in cDKO mice. After 1 hour pre-incubation of acute slices with 10 nM recAPPs α or 10 nM recAPPs α and 10 nM BTX fEPSPs were recorded. Hippocampal acute slices treated with 10 nM BTX and recAPPs α revealed significantly impaired induction (t20-25) and maintenance (t75-80) of LTP in comparison to slices of cDKO mice recorded in the presence of recAPPs α alone. **F, G** Co-application of BTX and CT α 16, the C-terminal domain of APPs α , significantly inhibits synaptic plasticity in cDKO mice. After 1 hour pre-incubation of acute slices with 10 nM CT α 16, or 10 nM CT α 16 and 10 nM BTX fEPSPs were recorded. Hippocampal acute slices treated with 10 nM BTX and CT α 16 revealed similar to recAPPs α , a significantly impaired induction (t20-25) and maintenance (t75-80) of LTP in comparison to slices of cDKO mice recorded in the presence of CT α 16 alone. Age: 5-6 months of age. n=number of recorded slices. N=number of animals. Data represent mean \pm SEM. Data were analysed by unpaired two-tailed Students t-test. *p<0.05, **p<0.01.

Figure 7: Potentiating effect of CT α 16 and APPs α on recombinant homomeric α 7-nAChRs.

A Nicotine- and acetylcholine-induced whole-cell current traces of α 7-nAChRs expressed in *Xenopus* oocytes recorded in the absence or presence of CT α 16 or CT α 16_{scr}, respectively. Note specific robust potentiation of nicotine- and acetylcholine-induced currents by CT α 16, but no direct activation of α 7-nAChRs by either peptide in the absence of agonist (not shown). Bars indicate application of

EC₅₀ agonist concentrations and of the peptide indicated (green: CT α 16: grey: CT α 16_{scr}). **B** Quantification of potentiation shows that CT α 16 enhances nicotine- and acetylcholine-induced currents to a similar extent whereas CT α 16_{scr} had no effect. **C** CT α 16 dose-response curve obtained with submaximal nicotine concentrations (100 μ M) with a corresponding EC₅₀ value of 10.7 ± 4.6 nM and a hill-coefficient of 2.1 ± 0.3 (n=4). **D** Nicotine-induced whole-cell current traces of α 7-nAChRs in the presence of 20 nM recAPPs α (green bar) or 20 nM recAPPs β (blue bar). Note that only recAPPs α efficiently potentiates α 7-nAChRs, which is blocked by BTX (orange bar). **E** Quantification of potentiation shows that recAPPs α enhances nicotine-induced currents to a similar extent as CT α 16 (see for comparison Figure 7B) while recAPPs β had no effect. **F** Nicotine dose-response curve obtained either in the presence of 20 nM recAPPs α (green circles, left) or without treatment (black circles, right). Note that recAPPs α treatment shifts the curve to the left, significantly reducing the apparent agonist affinity by about 2-fold (EC₅₀ of 40.3 ± 6.0 μ M, green curve vs. EC₅₀ of 80.5 ± 12.7 μ M, black curve; n=5; *p<0.05). For statistical evaluation of potentiation we performed a paired two-tailed Students t-test of the agonist-induced currents in the absence and presence of the indicated peptide. n=number of oocytes. Data represent mean \pm SEM. ^{ns}p>0.05, *p<0.05.

Expanded View Legends

EV1: AVV-Venus and AVV-APPs vectors mediate comparable neuron specific expression throughout the dorsal hippocampus. **A** Double immunostaining of CA1 pyramidal cells. APPs β (HA-tag, red) is exclusively expressed in neurons (NeuN, blue, left), but not in astrocytes (GFAP, blue, middle) or microglia (Iba1, blue, right). Scale bar: 20 μ m. **B** Expression was investigated by immunohistochemistry in different coronal sections from dorsal to ventral. **C** Venus, APPs α and APPs β (HA-tag) expression is shown for different sections of the hippocampus. Expression is absent in ventral portions of the hippocampus. Scale bar: 1 mm.

Figure EV2: APPs α and APPs β are transported through the secretory pathway and secreted efficiently. **A** Western blot analysis of lysate (L) and supernatant (SN) of pAAV-APPs α and pAAV-APPs β transfected HEK293T cells using an HA-tag specific antibody. Note the secretion of HA-APPs α and HA-APPs β into the cell supernatant. Mature APPs is posttranslationally modified and runs at slightly higher MW. **B** Western blot analysis of medium from cortical neurons transduced with AAV-APPs α or AAV-APPs β . 10⁵ cDKO neurons were transduced at DIV7 with 10⁴ genome copies per cell of either AAV-APPs α or AAV-APPs β . After 12 days medium was exchanged and neuronal supernatants were harvested on the next day. Equal amounts (2 μ l) of supernatant were subjected to capillary electrophoresis followed by immunodetection (WES system, ProteinSimple, USA). Note that similar amounts of HA-APPs α and HA-APPs β are secreted into the medium of transduced neurons. **C-E** Immunocytochemistry of neurons transduced with AAV-APPs α or AAV-APPs β neurons. Transduced neurons positive for the neuronal marker NeuN (red) were identified by Venus expression (green). **D, E** Confocal images of neurons stained with the ER marker Calreticulin (green), the Golgi marker Giantin (green) and α -HA staining to detect APPs (red). Note that both HA-APPs α and HA-APPs β show co-localization (white arrows) with the ER (**D**) and Golgi markers (**E**) indicating successful transport through the secretory pathway. Scale bars: 100 μ m (**C**), 10 μ m (**D,E**).

EV3: Basal transmission in cDKO mice treated with APPs α or APPs β is not altered compared to LM control animals injected with Venus.

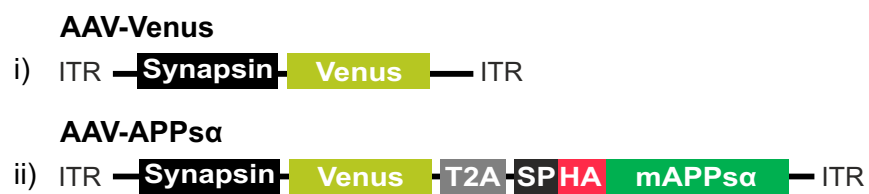
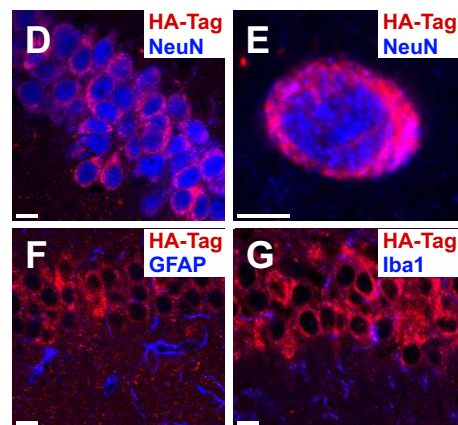
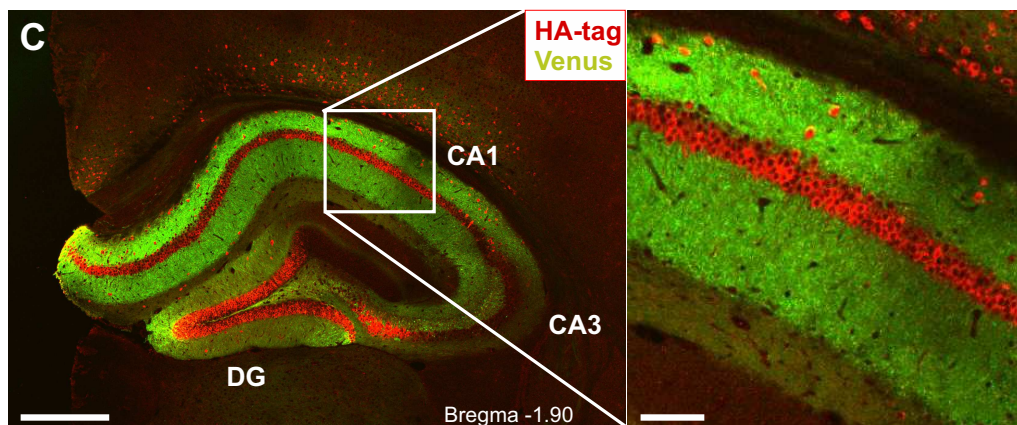
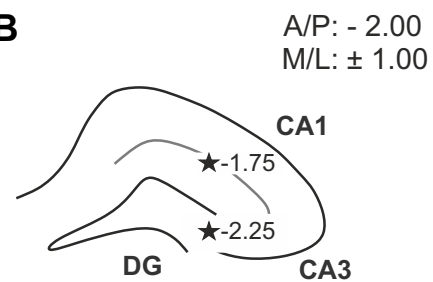
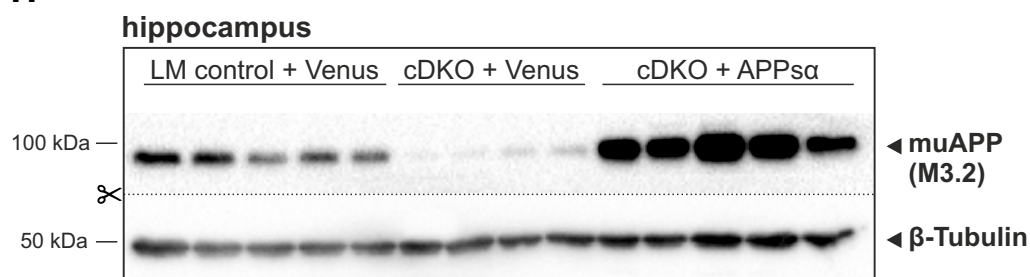
A, C Neuronal excitability is comparable at all stimulus intensities (25-250 μ A) between all groups injected with the indicated AAV vectors. **B, D** No significant alterations can be detected when analyzing the Input-Output (IO) strength of the viral vector injected groups of mice at any fiber volley (FV) amplitude.

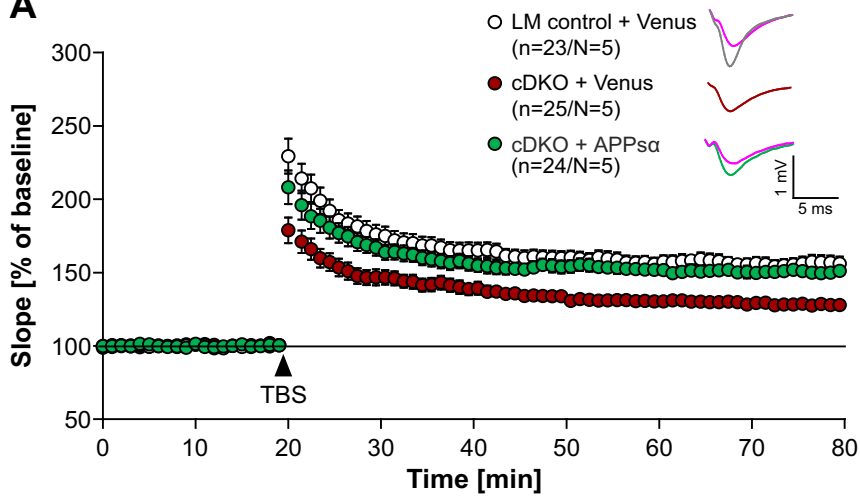
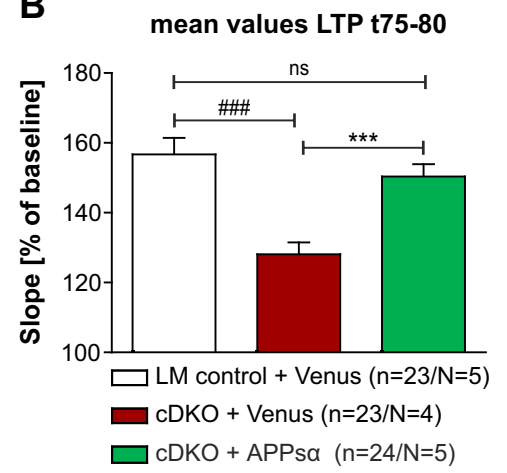
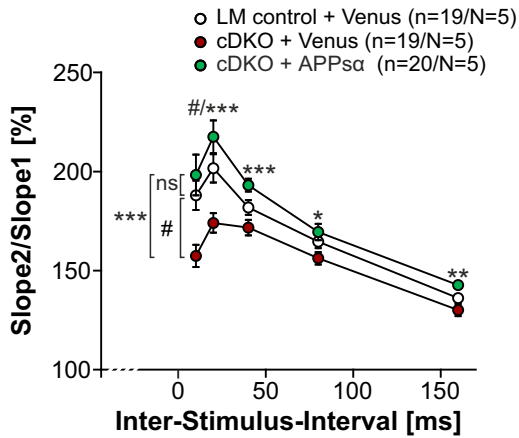
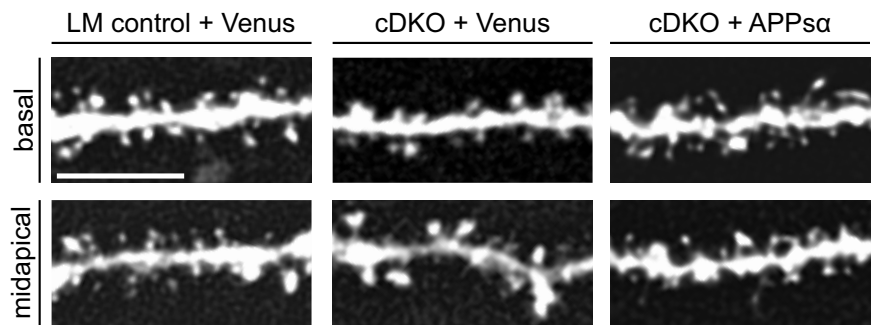
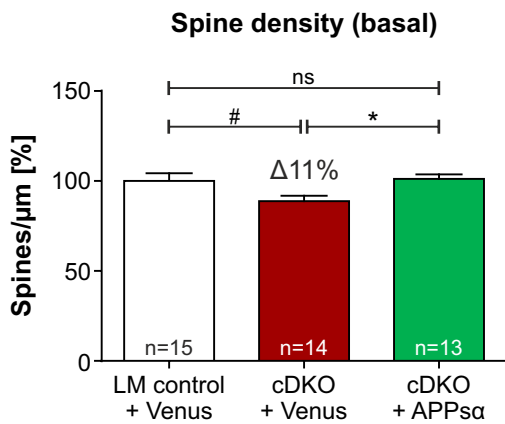
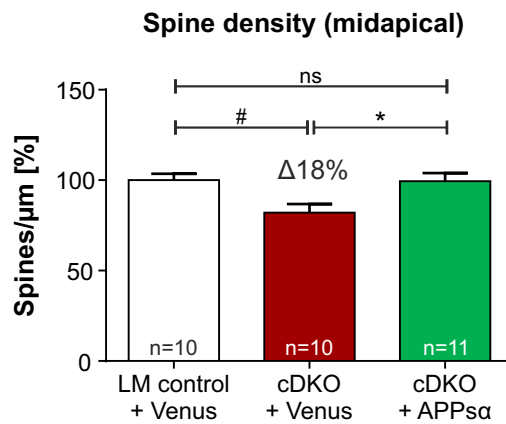
EV4: Inhibition of α 7-nAChRs by BTX after APPs α pre-incubation does not inhibit LTP **A** Experimental set-up: pre-application of APPs α or CT α 16 before addition of 10 mM Bungarotoxin (BTX) 30 min prior to TBS (arrowhead). **B, C** Hippocampal acute slices treated with APPs α for 1 h and subsequent addition of 10 nM BTX did not significantly impair induction (t20-25) and maintenance of LTP (t75-80) in comparison to slices of cDKO mice recorded in the presence of APPs α alone.

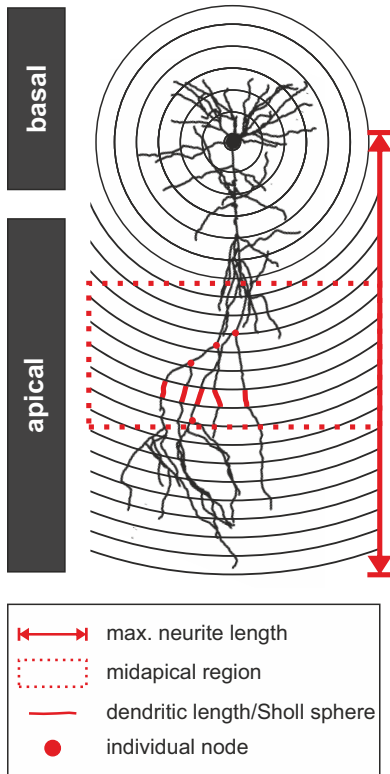
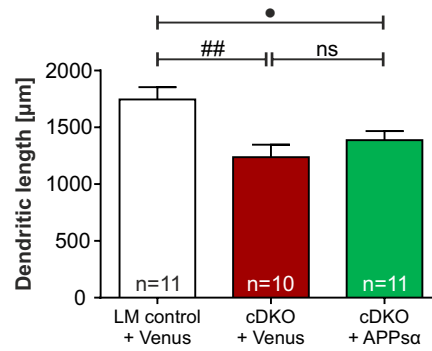
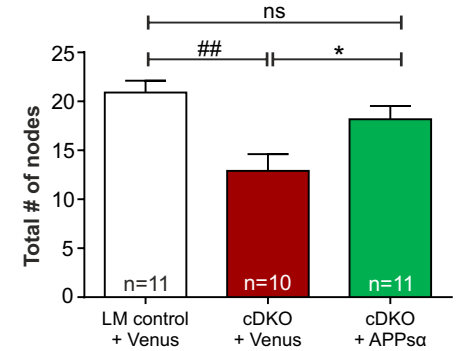
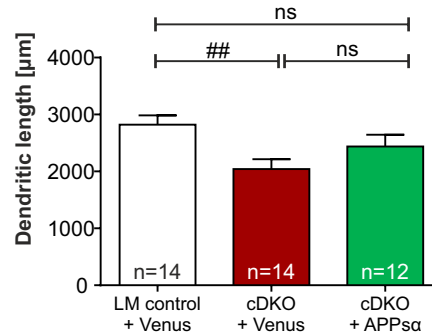
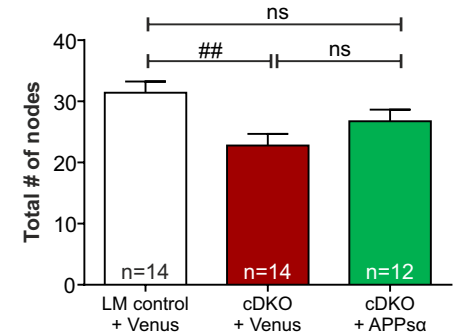
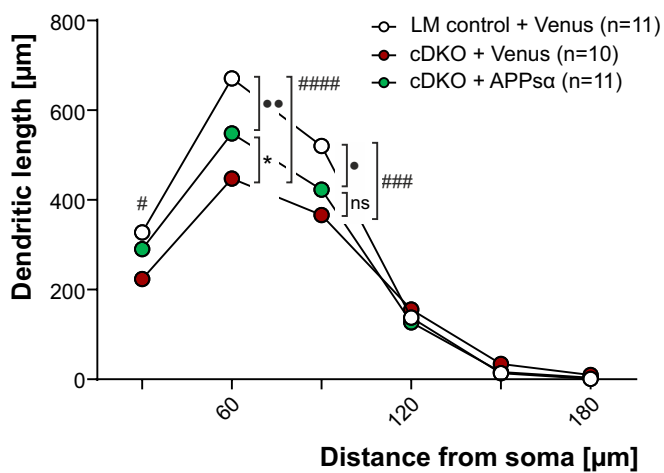
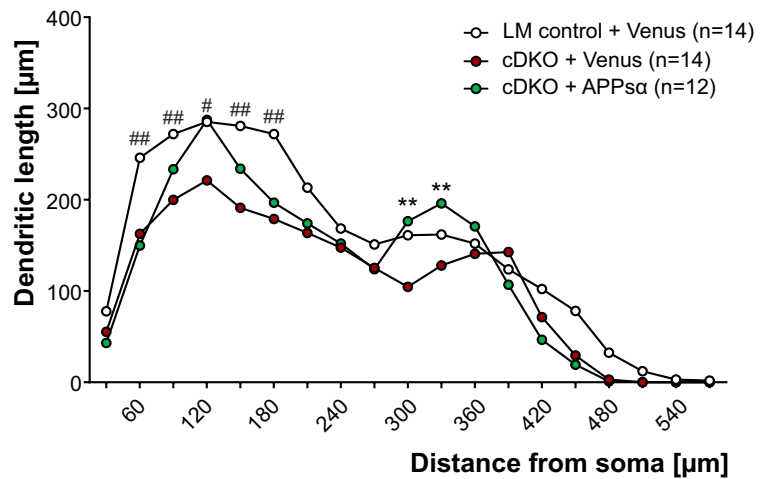
D, E The treatment with CT α 16 for 1 h and subsequent addition of 10 nM BTX did not significantly impair induction (t20-25) or maintenance of LTP (t75-80). Age: 5-6 months of age. n=number of recorded slices, N=number of animals. Data represent mean \pm SEM. Data were analysed by unpaired two-tailed Students t-test. ^{ns}p>0.05.

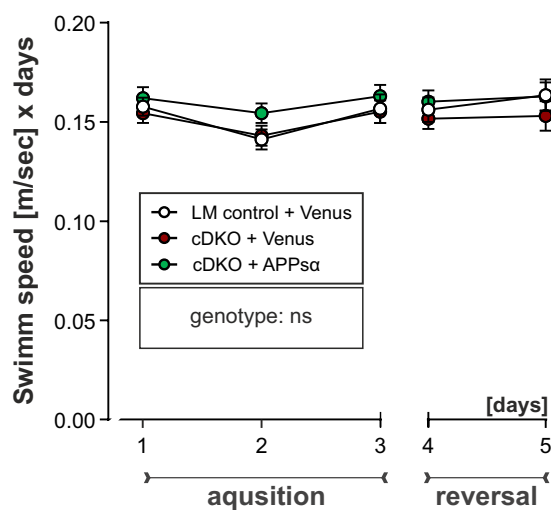
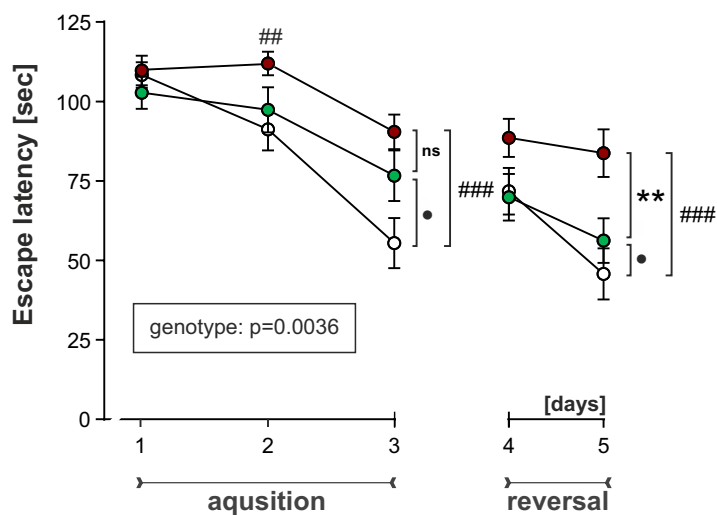
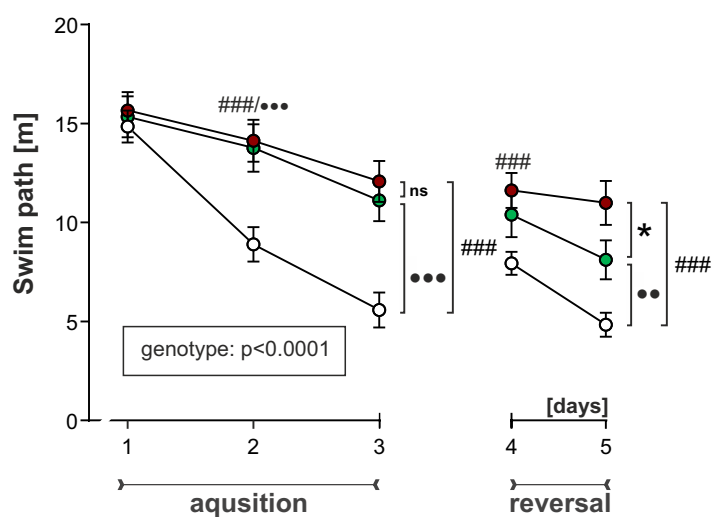
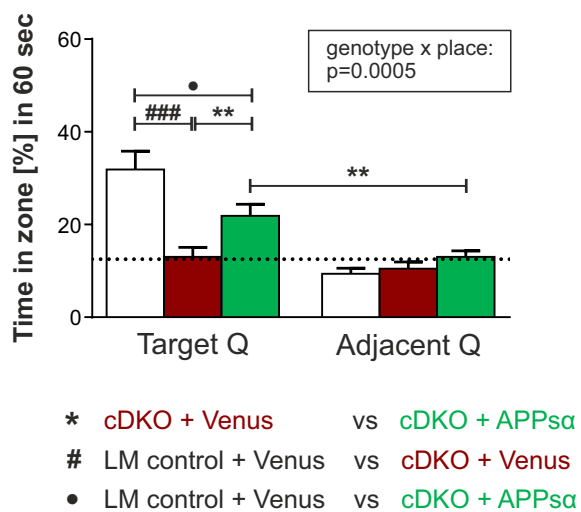
EV5: Neither CT α 16 nor APP α potentiate the homomeric α 1 glycine receptor.

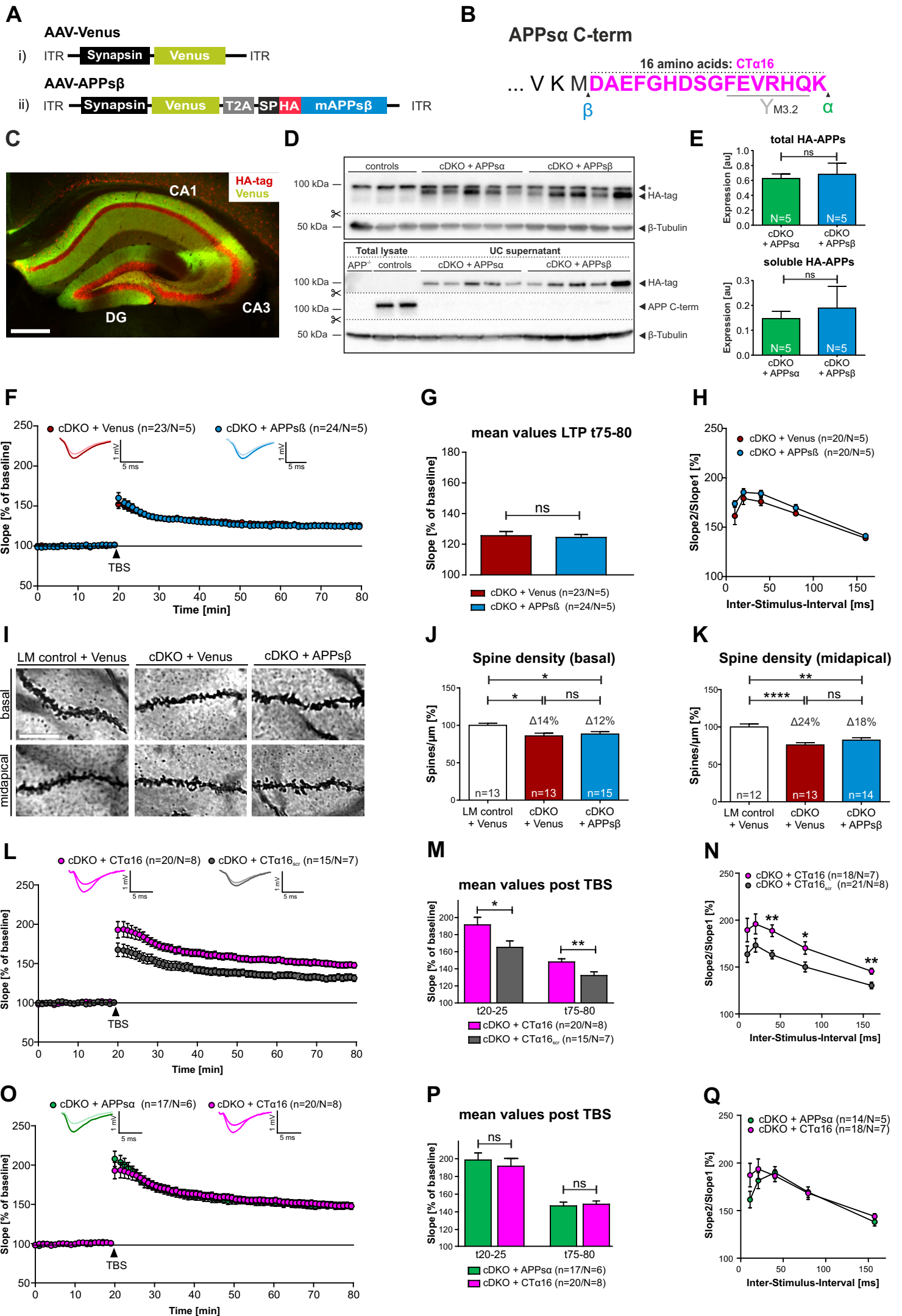
A Glycine-induced whole-cell current traces of homomeric α 1 glycine receptor (GlyR) expressed in *Xenopus* oocytes recorded in the absence or presence of CT α 16 or APP α , respectively. No direct activation of α 1-GlyR by CT α 16 or APP α in the presence of the agonist was detected (not shown). Bars indicate application of EC₅₀ glycine concentrations and of the peptide indicated. **B** Quantification of potentiation shows that neither CT α 16 nor APP α effect glycine-induced currents. Data represent mean \pm SEM. Data were analysed by paired two-tailed Students t-test. ^{ns}p>0.05.

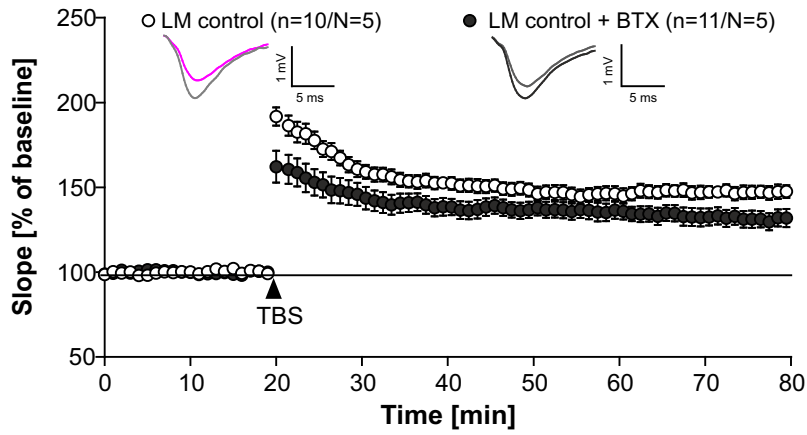
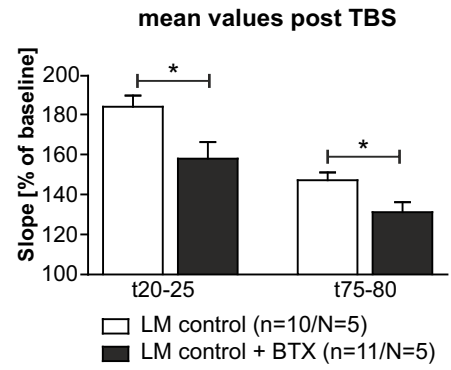
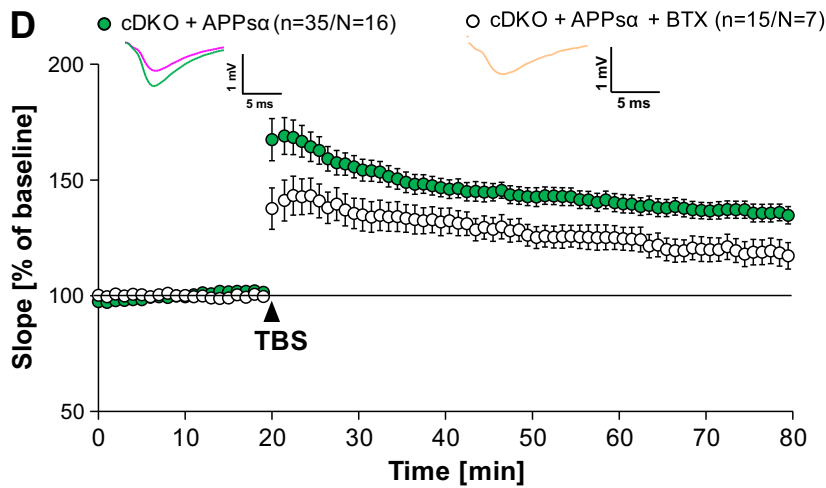
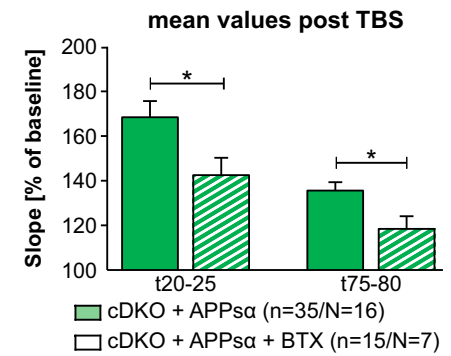
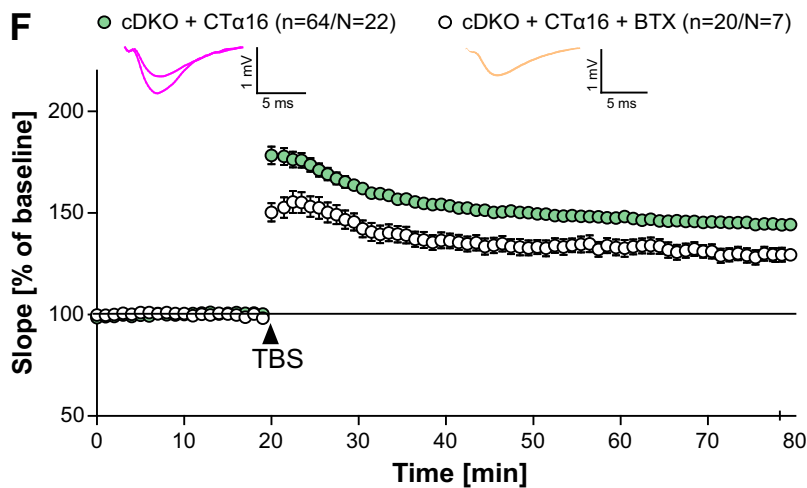
A**B****H**

A**B****C****D****E****F**

A**LM control + Venus****cDKO + Venus****cDKO + APPsα****B****C****Total dendritic length (basal)****D****Total dendritic branching (basal)****E****Total dendritic length (apical)****F****Total dendritic branching (apical)****G****Sholl analysis - Dendritic length (basal)****H****Sholl analysis - Dendritic length (apical)**

A**Swim speed****B****Escape latency****C****Swim path****D****Probe Trial - Zone time**



A**B****C****D****E****F****G**